

RESEARCH ARTICLE

The development of extracellular vesicle markers for the fungal phytopathogen *Colletotrichum higginsianum*

Brian D. Rutter¹  | Thi-Thu-Huyen Chu^{2,3}  | Jean-Félix Dallery²  | Kamil K. Zajt¹  |
Richard J. O'Connell²  | Roger W. Innes¹ 

¹Department of Biology, Indiana University, Bloomington, Indiana, USA

²Université Paris-Saclay, INRAE, UR BIOGER, Thiverval-Grignon, France

³University of Science and Technology of Hanoi, Vietnam Academy of Science and Technology, Hanoi, Vietnam

Correspondence

Brian D. Rutter, Department of Biology, Indiana University, Bloomington, IN 47405, USA.
Email: brutter@iu.edu

Funding information

Saclay Plant Sciences-SPS, Grant/Award Number: ANR-17-EUR-0007; Agence Nationale de la Recherche, Grant/Award Number: ANR-17-CAPS-0004-01; National Science Foundation, Grant/Award Numbers: IOS-1645745, IOS-1842685; U.S. Department of Energy (DOE) Office of Biological and Environmental Research, Grant/Award Number: DE-SC0020348

Abstract

Fungal phytopathogens secrete extracellular vesicles (EVs) associated with enzymes and phytotoxic metabolites. While these vesicles are thought to promote infection, defining the true contents and functions of fungal EVs, as well as suitable protein markers, is an ongoing process. To expand our understanding of fungal EVs and their possible roles during infection, we purified EVs from the hemibiotrophic phytopathogen *Colletotrichum higginsianum*, the causative agent of anthracnose disease in multiple plant species, including *Arabidopsis thaliana*. EVs were purified in large numbers from the supernatant of protoplasts but not the supernatant of intact mycelial cultures. We purified two separate populations of EVs, each associated with over 700 detected proteins, including proteins involved in vesicle transport, cell wall biogenesis and the synthesis of secondary metabolites. We selected two SNARE proteins (Sncl and Sso2) and one 14-3-3 protein (Bmh1) as potential EV markers and generated transgenic strains expressing fluorescent fusions. Each marker was confirmed to be protected inside EVs. Fluorescence microscopy was used to examine the localization of each marker during infection on *Arabidopsis* leaves. These findings further our understanding of EVs in fungal phytopathogens and will help build an experimental system to study EV interkingdom communication between plants and fungi.

KEYWORDS

14-3-3 proteins, *Colletotrichum higginsianum*, extracellular vesicles, phytopathogen, protoplasts, SNARE proteins

1 | INTRODUCTION

Secretory pathways are essential to the life of a fungus. They contribute to the synthesis and remodelling of cell walls, nutrient acquisition and host/symbiont interactions (Krijger et al., 2014; Latge, 2007; McCotter et al., 2016). In particular, plant fungal pathogens rely heavily on secreted proteins to invade and manipulate their hosts. Compared to saprophytes and animal pathogens, phytopathogens have considerably larger secretomes (Krijger et al., 2014). While the composition of these secretomes varies depending on the infection strategy, many phytopathogens secrete cell wall-degrading enzymes to facilitate penetration into plant tissues and nutrient uptake (Kubicek et al., 2014). They also secrete small protein effectors that function in the plant apoplast or cytoplasm to favour fungal infection, for example by masking chitin from detection by plant immune receptors (de Jonge et al., 2010; van Esse et al., 2007), by inhibiting or modifying plant antimicrobial enzymes, such as chitinases, proteases and peroxidases (Hemetsberger et al., 2012; Jashni et al., 2015; Naumann & Price, 2012; Naumann & Wicklow, 2010; Naumann et al.,

This is an open access article under the terms of the [Creative Commons Attribution](https://creativecommons.org/licenses/by/4.0/) License, which permits use, distribution and reproduction in any medium, provided the original work is properly cited.

© 2022 The Authors. *Journal of Extracellular Vesicles* published by Wiley Periodicals, LLC on behalf of the International Society for Extracellular Vesicles.

2009; Naumann et al., 2011; van Esse et al., 2008), or by suppressing plant defence signalling and immune responses (Pradhan et al., 2021). In addition to proteins, phytopathogens can also secrete secondary metabolites capable of damaging host tissues or interfering with plant defences and associated signalling pathways (Collemare et al., 2019; Peng et al., 2010).

Most extracellular proteins are released through the conventional secretory pathway, in which proteins possessing an N-terminal signal peptide are trafficked from the endoplasmic reticulum (ER) to the Golgi and then delivered inside secretory vesicles to the plasma membrane (PM) for release outside the cell (Peberdy, 1994; Shoji et al., 2014). While the conventional pathway is the best studied route for secreted proteins, there are alternative, unconventional pathways. Proteins can be secreted directly across the PM through pores or via ABC-transporters, and some secretory vesicles released from the ER can bypass the Golgi apparatus completely (Rabouille, 2017). Proteins can also be released within extracellular vesicles (EVs), nano-sized, lipid-bilayer compartments that function in the extracellular transport of proteins, lipids, nucleic acids and other macromolecules (Rodrigues et al., 2013; Shoji et al., 2014). EVs can pinch off directly from the PM or form inside late endosomes (multivesicular bodies) as intraluminal vesicles that are released upon fusion of the late endosome with the PM (van Niel et al., 2018).

Although the majority of EV research has been conducted in mammalian systems, the phenomenon of EV secretion has been observed in all domains of life (Woith et al., 2019; Yanez-Mo et al., 2015). Fungal EVs were first isolated in 2007 from the opportunistic human pathogen *Cryptococcus neoformans* and have since been isolated from multiple species of yeasts and filamentous fungi (Rizzo et al., 2020; Rodrigues et al., 2007). Fungal EVs contain a diverse cargo of lipids, polysaccharides and secondary metabolites. They are enriched for proteins involved in cellular metabolism, translation, transport, signalling and stress responses (Bleackley et al., 2019). Similar to mammalian EVs, fungal EVs also contain a variety of RNA molecules, including small, noncoding and messenger RNAs (Peres da Silva et al., 2015).

Functionally, fungal EVs have been described as “virulence bags” containing multiple factors important for pathology (Albuquerque et al., 2008; Matos Baltazar et al., 2016; Rodrigues et al., 2007; Vallejo et al., 2012; Vargas et al., 2015). Injections of fungal EVs in mice have been shown to enhance the virulence of fungal pathogens and promote the colonization of organs (Huang et al., 2012; Ikeda et al., 2018; Marina et al., 2020). Through cell-to-cell communication, fungal EVs also promote biofilm formation, antibiotic resistance and heightened virulence states in recipient fungal cells (Hai et al., 2020; Zarnowski et al., 2018).

Fungal EVs have also been linked to cell wall synthesis. Under conditions that stimulate the regeneration of the cell wall, protoplasts of *Aspergillus fumigatus* release high numbers of EVs. These EVs are associated with carbohydrates and proteins essential for the synthesis of major cell wall components (ex: β -1,3- and α -1,3-glucans, chitin, galactomannan and galactosaminogalactan) (Rizzo et al., 2020). EVs of *Saccharomyces cerevisiae* are also associated with glucan and chitin synthases. The presence of these proteins as EV cargo allows the vesicles to rescue yeast cells treated with an inhibitor of β -1,3-glucan synthesis (Zhao et al., 2019). It has been suggested that the cell wall remodelling capabilities of EVs facilitate their passage through the fungal cell wall to reach the extracellular space, but this has not yet been fully verified (Rizzo et al., 2020).

While the majority of fungal EV studies have focused on human pathogens, there is a growing body of research on plant pathogens. In fact, the first example of EVs isolated from a filamentous fungus came from *Alternaria infectoria*, the causative agent of black point and leaf blight diseases in grain crops (Silva et al., 2014). More recent studies have examined EVs from *Zymoseptoria tritici* (septoria leaf blotch in wheat), *Fusarium oxysporum* f. sp. *vasinfectum* (*Fusarium* wilt disease in cotton), *Ustilago maydis* (maize smut) and *Fusarium graminearum* (*Fusarium* stalk rot) (Bleackley et al., 2019; Garcia-Ceron et al., 2021; Garcia-Ceron et al., 2021; Hill & Solomon, 2020). EVs from these phytopathogens resemble other fungal EVs in their size and contents. They are enriched for proteins involved in primary cellular metabolism and can contain full-length mRNAs (Bleackley et al., 2019; Hill & Solomon, 2020; Kwon et al., 2021; Silva et al., 2014). EVs from *F. oxysporum* f. sp. *vasinfectum* also copurify on a density gradient with a phytotoxic, purple-coloured metabolite that causes tissue collapse when injected into leaves of cotton plants or *Nicotiana benthamiana* (Bleackley et al., 2019). In all cases, the EVs from fungal phytopathogens are postulated to promote virulence (Bleackley et al., 2019; Kwon et al., 2021; Silva et al., 2014).

While research into fungal EVs is growing, questions regarding their biogenesis, ultimate functions and ability to cross the fungal cell wall remain unanswered. Researchers have also struggled to define fungal EV biomarkers. Tetraspanin proteins such as CD63 are widely used as EV markers in mammalian systems (Choi et al., 2015). While lacking true orthologs to human tetraspanins, filamentous fungi do encode proteins having a very similar domain structure, namely, four transmembrane domains, an intracellular loop and two extracellular loops, the larger of which contains the highly conserved CCG cysteine pattern that is a hallmark of mammalian tetraspanins (Lambou et al., 2008). However, these fungal tetraspanins have so far not been detected in any fungal EV proteomes. Similarly, although fungi possess orthologs to components of the ESCRT complex, another common mammalian EV marker, they are often present in low abundance or not detectable in fungal EVs (Bleackley et al., 2019). A further problem is that fungal EVs are rarely density-gradient purified. This means that the majority of published fungal EV proteomes, sources for selecting biomarkers, likely contain copelleting, extravesicular molecules.

In this study, we expand the current knowledge of fungal EVs by isolating EVs from the phytopathogen *Colletotrichum higginsianum*. Members of the genus *Colletotrichum* cause anthracnose leaf spot diseases on thousands of plant species and are mostly hemibiotrophic pathogens, meaning that they initially invade and derive nutrients from living plant cells (biotrophy) before later switching to a destructive necrotrophic phase, when they feed on dead host cells (O’Connell et al., 2012). *C. higginsianum* is

adapted to infect cruciferous plants, including not only crop species but also the model plant *Arabidopsis thaliana*. The pathosystem formed between these two organisms is regarded as a model for hemibiotrophic plant-fungus interactions (O'Connell et al., 2004). Here, we report that *C. higginsianum* is also capable of producing EVs. These EVs are not readily released from vegetative mycelia grown in liquid media, but they can be isolated in large numbers after removal of the cell wall. Two separate populations of EVs were purified from *C. higginsianum* protoplasts based on their buoyant density. Proteomic analysis of density gradient-purified vesicles revealed several hundred proteins, including those involved in cell wall synthesis/remodelling and the production of secondary metabolites. We further developed transgenic, fluorescent EV biomarker strains that could be used in the future to track EV release during infection. This research will strengthen fungal EV research and lay the groundwork for modelling interkingdom EV communication in plant-fungal interactions.

2 | MATERIALS AND METHODS

2.1 | Fungal material

Colletotrichum higginsianum isolate IMI349063A was used for all experiments including generation of transgenic strains. Stocks of fungal spores were stored in 15% glycerol and 1X potato dextrose broth at -80°C . Cultures were prepared fresh from stock and grown on 100 ml of Mathur's agar (2.8 g/L glucose, 2.2 g Mycological peptone, 1.2 g/L $\text{MgSO}_4 \times 7\text{H}_2\text{O}$, 2.7 g/L KH_2PO_4 , 30 g/L agar, pH 5.5) in 250 ml flasks. To create liquid cultures, spores from 7 to 14-day old cultures were collected from the surface of solid media into sterile, deionized water. Spores were inoculated at a final concentration of 5×10^5 spores/ml in liquid Mathur's medium. Liquid cultures (200–500 ml) were grown in the dark at 25°C and 100 rpm for 3 days.

2.2 | Transmission electron microscopy (TEM)

Hypocotyl segments (7 cm) were excised from 6-day-old seedlings of *Phaseolus vulgaris* cv. Kievitsboon KoeKoe and the cut ends were sealed with paraffin wax. The segments were placed horizontally on glass supports over wet paper inside plastic boxes, then inoculated with droplets (7 μl) of *C. lindemuthianum* spore suspension (5×10^5 spores/ml) and incubated at 17°C . At 4 days after inoculation, strips of hypocotyl tissue (c. 0.5 mm thick and 5 mm long) were cut parallel to the hypocotyl surface with a razor blade. Infected areas were excised using a 2 mm diameter biopsy punch and vacuum-infiltrated with 1-hexadecene, before mounting in 1-hexadecene between two aluminium sample holders (0.3 mm deep) and cryo-fixing in a Balzers HPM 010 high-pressure freezer. Tissues were freeze-substituted with acetone containing 2% (w/v) osmium tetroxide at -90°C for 48 h, -60°C for 12 h, and -30°C for 8 h using a Reichert CS freeze-substitution device. Samples were then infiltrated with Epon-Araldite resin and polymerized at 60°C . Ultrathin sections were mounted on Formvar-coated slot grids, stained with uranyl acetate and lead citrate, and viewed with a Hitachi H7000 TEM. Biotrophic hyphae of *C. higginsianum* were isolated from infected *A. thaliana* leaves by fluorescence-activated cell sorting, cryo-fixed and prepared for TEM as described previously (Takahara et al., 2009). The mean diameter and size ranges of vesicles observed using TEM were measured using ImageJ software.

For negative staining, vesicles resuspended in 20 mM Tris-HCl pH 7.5 were applied to glow-discharged 3.05-mm copper Formvar-carbon-coated electron microscopy grids (Electron Microscopy Sciences). After 1 min, samples were wicked off using filter paper, and the grids were washed with 2% uranyl acetate. The grids were allowed to air dry and imaged at 80 kV using a JEM-1010 transmission electron microscope (JEOL USA).

2.3 | Protoplast generation

For protoplast generation, mycelia from 3-day old liquid cultures were harvested by straining the culture through Miracloth (Millipore Sigma catalogue number 475855). The mycelia were transferred to a 50 ml Falcon tube and washed twice in 0.7 M NaCl by pelleting mycelia at 8,000 rpm and 25°C for 5 min using a JA25.50 rotor and resuspending in sterile saline solution. After the final wash, mycelia were added to a cell wall digestion solution (0.7 M NaCl, 10 mM phosphate buffer, 100 mg/ml VinoTaste Pro (Novozymes), pH 5.5) and allowed to acclimate for 10 min with gentle rocking. The fungi and cell wall digestion solution were then added to a 100 ml flask and incubated for 3 h at 25°C and 80 rpm. After digestion, samples of the solution were observed using a light microscope to verify the majority (> 95%) of observed fungal cells were converted from filamentous hyphal cells into spherical protoplasts. Protoplasts were then pelleted at 2,000 rpm and 4°C for 8 min using a JA25.50 rotor. The supernatant was transferred to a fresh 50 ml Falcon tube and the pelleting step was repeated to remove any residual protoplasts. The supernatant was then filtered through a 0.22 μm filter and kept on ice. Pelleted protoplasts were resuspended in cold, sterile 0.7 M NaCl.

Their viability was assessed by mixing with Evans Blue to a final concentration of 0.01% (w/v) and examining protoplasts for dye uptake using a light microscope.

2.4 | Crude EV isolation

Extracellular vesicles were isolated from the supernatant of cell wall digestion reactions using differential ultracentrifugation. After filtration, 12 ml samples were added to 14 × 89 mm ultraclear centrifuge tubes (Beckman Coulter, Inc., Brea, CA, USA) and centrifuged at 10,000 g and 4 °C for 30 min (SW41 rotor, Optima XPN-100 ultracentrifuge; Beckman Coulter, Inc.) to remove any potential large debris. The majority of the supernatant (11.5 ml) was transferred to a fresh tube using a pipette, the volume was brought up to 12 ml using fresh 0.7 M NaCl and the EVs were pelleted at 60,000 g and 4 °C for 90 min (SW41, Optima XPN-100 ultracentrifuge). After this step, 11.5 ml of supernatant was removed using a pipette, and the pellet was resuspended in the remaining 0.5 ml. The EV sample was then transferred to a smaller 13 × 51 mm polycarbonate ultracentrifugation tube (Beckman Coulter, Inc., Brea, CA, USA), brought up to 3 ml using sterile 20 mM Tris-HCl pH 7.5 and pelleted at 40,000 g and 4 °C for 60 min (TLA100.3 rotor, Optima Max-XP ultracentrifuge, Beckman Coulter, Inc.). Finally, the supernatant was completely decanted, the upper 3/4 of the tubes were dried with a Kim Wipe to remove residual liquid.

2.5 | Density purification

Extracellular vesicles were further purified on a discontinuous iodixanol gradient (Optiprep; Sigma-Aldrich) consisting of 40% (v/v), 20% (v/v), 10% (v/v), and 5% (v/v) iodixanol layers. The EV pellets were resuspended in 1 ml of 20 mM Tris-HCl pH 7.5 and mixed with 2 ml of 60% Optiprep (Sigma-Aldrich, St. Louis, MO, USA) to create a 40% layer. The remaining layers were created by diluting a 60% OptiPrep stock solution in 20 mM Tris-HCl pH 7.5. The gradient was formed by sequentially adding each 3 ml layer to a 14 × 89 mm ultraclear centrifuge tube (Beckman Coulter, Inc.), starting with the 40% solution and ending with the 5% solution. The gradient was centrifuged for 17 h at 100,000 g and 4 °C (SW41, Optima XPN-100 ultracentrifuge). After centrifugation, the top 3 ml were discarded. The next six 1 ml fractions were collected for further analysis. Samples were added to 13 × 51 mm polycarbonate ultracentrifugation tubes (Beckman Coulter, Inc., Brea, CA) and brought up to a volume of 3.5 ml using cold, sterile 20 mM Tris-HCl pH 7.5. Samples were centrifuged for 1 h at 100,000 g and 4 °C (TLA100.3, Optima Max-XP ultracentrifuge). The supernatant was completely decanted, the upper 3/4 of the tubes were dried with a Kim wipe to remove residual liquid and the pellet was resuspended in 20 mM Tris-HCl pH 7.5.

2.6 | NanoParticle tracking analysis

EV sample particle concentrations and diameters were determined using a ZetaView Particle Tracking Analyzer (Particle Metrix, Diessen) and associated software. The machine was calibrated using 100 nm polystyrene beads, and samples were diluted in 1 ml of 20 mM Tris-HCl, pH 7.5. The machine operated under the following settings: max. diameter: 500 nm, min. diameter: 5 nm, min. brightness: 20, shutter speed: 100.

2.7 | Mass spectrometry (MS) analysis

Vesicle pellets were resuspended in 20 μ l of buffer containing 8 M urea and diluted to a final volume of 160 μ l using 100 mM ammonium bicarbonate, for a final urea concentration of 1 M. Disulfide bonds were reduced by incubation for 45 min at 57 °C with a final concentration of 10 mM Tris (2-carboxyethyl) phosphine hydrochloride (Catalogue no C4706, Sigma Aldrich). A final concentration of 20 mM iodoacetamide (Catalogue no I6125, Sigma Aldrich) was then added to alkylate these side chains and the reaction was allowed to proceed for 1 h in the dark at 21 °C. A total of 500 ng trypsin was added (V5113, Promega) and the samples were digested for 14 h at 37 °C. The following day, the sample was dried down and resuspended in 30 μ l 0.1% formic acid, then desalted using a zip tip (EMD Millipore).

Samples were analysed by LC-MS on an Orbitrap Fusion Lumos (ThermoFisher) equipped with an Easy NanoLC1200 HPLC (ThermoFisher). Peptides were separated on a 75 μ m × 15 cm Acclaim PepMap100 separating column (Thermo Scientific) downstream of a 2 cm guard column (Thermo Scientific). Buffer A was 0.1% formic acid in water. Buffer B was 0.1% formic acid in 80% acetonitrile. Peptides were separated on a 120 min gradient from 4% B to 33% B. Peptides were collisionally fragmented using HCD mode. Precursor ions were measured in the Orbitrap with a resolution of 120,000. Fragment ions were measured in the ion trap. The spray voltage was set at 1.8 kV. Orbitrap MS1 spectra (AGC 4 × 10⁵) were acquired from 400 to 2000 m/z followed by data-dependent HCD MS/MS (collision energy 30%, isolation window of 2 Da) for a three second cycle time. Charge state

screening was enabled to reject unassigned and singly charged ions. A dynamic exclusion time of 60 s was used to discriminate against previously selected ions.

2.8 | Database search

The LC-MS/MS data was searched using Proteome Discoverer 2.5 (ThermoFisher Scientific). MS spectra were searched against a *Colletotrichum higginsianum* database downloaded from Uniprot on 06/2018. The database search parameters were set as follows: two missed tryptic cleavage sites were allowed for trypsin digested with 10 ppm precursor mass tolerance and 0.05 Da for fragment ion quantification tolerance. Oxidation of methionine was set as a variable modification. Carbamidomethylation (C; +57 Da) was set as a static modification. Results were filtered using the Percolator node with a FDR of 0.01.

2.9 | Analysis of protein sequences

Protein sequences were analyzed for predicted signal peptides using SignalP - 5.0 (<https://services.healthtech.dtu.dk/service.php?SignalP-5.0>, Almagro Armenteros et al., 2019). Transmembrane regions were predicted using TMHMM - 2.0 (<https://services.healthtech.dtu.dk/service.php?TMHMM-2.0>, Krogh et al., 2001, Sonnhammer et al., 1998). GO term enrichment was determined using FungiFun2 (Priebe et al., 2015).

2.10 | Immunoblots

For immunoblots, 40 μ l of resuspended vesicles in 20 mM Tris-HCl, pH 7.5 were combined with 10 μ l of 5X SDS loading buffer (250 mM Tris-HCl, pH 6.8, 8% SDS, 0.1% Bromophenol Blue, 40% glycerol, and 400 mM dithiothreitol) and incubated at 95°C for 5 min. Protoplast lysate samples were used as positive controls. Pelleted protoplasts were frozen in liquid nitrogen and ground into a powder using a mortar and pestle. Proteins from the ground protoplasts were extracted in 500 μ l of protein extraction buffer (150 mM NaCl, 50 mM Tris HCl, pH 7.5, 0.1% Nonidet P-40, and 1% protease inhibitor cocktail [Sigma-Aldrich, Catalogue No.: P2714]) and centrifuged for 5 min at 10,000 rpm and 4°C. Forty microliters of supernatant were combined with 10 μ l of 5X SDS loading buffer, and the mixture was incubated at 95°C for 5 min. Protein concentrations were determined using Pierce 660 nm Protein Assay Reagent (ThermoFisher Scientific). Samples were loaded on 4% to 20% Precise Protein Gels (ThermoFisher Scientific) and separated at 120 V for ~1 h in BupH Tris-HEPES-SDS running buffer (ThermoFisher Scientific). The proteins were transferred to a nitrocellulose membrane (GE Water and Process Technologies). Total protein was visualized with a quick Ponceau S stain. Membranes were washed with 1X Tris-buffered saline containing Tween 20 (TBST; 50 mM Tris-HCl and 150 mM NaCl, pH 7.5, 0.1% Tween 20) and blocked with 5% Difco Skim Milk (BD) overnight at 4°C with gentle rocking. Membranes were incubated with rabbit anti-RFP (Abcam, Catalogue No.: ab62341) or anti-NeonGreen antibody (Chromotek, Catalog No.: 32F6) each at a 1:1,000 dilution or anti-SOD2 (ABclonal, Catalogue No.: A1340) at 1:500 for 1 h, washed with TBST, and incubated with horseradish peroxidase-labelled goat antirabbit antibody (Abcam, Catalogue No.: ab6721) at a 1:5,000 dilution for 1 h. After a final wash in TBST, protein bands were imaged using Immuno-Star Reagents (Bio-Rad) and X-ray film. Band intensities were quantified using ImageJ V2.0.0-rc-43/1.52n.

2.11 | Protease protection assay

For protease protection assays, crude EV pellets were resuspended in 150 mM Tris-HCl, pH 7.8 and divided into three equal samples. Sample A was treated with buffer only. Sample B was treated with 1 μ g/ml trypsin (Promega). Sample C was pretreated with 1% Triton X-100 (EMD-Millipore) followed by treatment with 1 μ g/ml trypsin (Promega). Triton X-100 treatment was carried out on ice for 30 min. Trypsin treatment was carried out at 25 °C for 1 h. All samples were subjected to the same incubation temperatures and times.

2.12 | Molecular cloning and fungal transformation

Predicted cDNA sequences of putative EV marker genes were amplified from the genomic DNA of *Colletotrichum higginsianum* isolate IMI 349063A including *ChSnc1* (protein ID: OBR08408.1, gene ID: CH63R_07173), *ChSso2* (protein ID: OBR07592.1, gene ID: CH63R_09113) and *ChBmh1* (protein ID: OBR15797.1, gene ID: CH63R_00977). All cloning fragments were amplified by PCR using Phusion High-Fidelity DNA polymerase (Thermo Scientific). Plasmids with *ChSnc1* and *ChSso2* insertions were

made using *in vivo* assembly by homologous recombination in *E. coli*. *ChSnc1* was tagged with the *mScarlet-I* sequence at its 5' terminus under the control of its native promoter and cloned into the *SmaI*-digested pBIG4MRH binary vector (Tanaka et al., 2007). *ChSso2* was tagged with the *mNeonGreen* sequence at its 5' terminus under the *ChActin* (Gene ID: CH63R_04240) promoter consisting of 1.7 kb upstream of the start codon; fragments were cloned into *XmnI*-digested pCGEN plasmid (Motteram et al., 2011). *ChBmh1* was fused to *mCherry* as a C-terminal tag with an intervening linker sequence *ggtcccgggggatcc* and placed under the *ChActin* promoter. The fragments were assembled together with the *SmaI*-digested pBIG4MRH vector using the NEBuilder HiFi DNA Cloning kit according to the manufacturer's instructions (New England Biolabs). The primers used are summarized in Table S7. Recombinant DNA plasmids were inserted in electrocompetent cells of *Agrobacterium tumefaciens* strain C58C1 then transformed into *C. higginsianum* isolate IMI349063A using *Agrobacterium tumefaciens*-Mediated Transformation (ATMT) (Huser et al., 2009). Transformants of *ChSnc1* and *ChBmh1* were selected on potato dextrose agar (PDA) supplemented with hygromycin (100 $\mu\text{g/ml}$), while *ChSso2* selection was performed on PDA supplemented with geneticin (300 $\mu\text{g/ml}$).

2.13 | Fungal inoculation and confocal microscopy

To determine the subcellular localization of fluorescent fusion proteins in hyphae growing *in vitro*, fungal transgenic strains were grown on Mathur's agar plates for 3 days at 25°C. Samples were prepared using the "inverted agar block method" (Hickey et al., 2004). A block of agar was cut from the edge of a colony and mounted upside down in a drop of Mathur's liquid medium on a glass-bottomed Petri dish. For protein localization *in planta*, droplets of fungal spore suspension (5×10^5 spores/ml) were inoculated on cotyledons of 11- to 12-day-old seedlings of *Arabidopsis thaliana* accession Col-0. Seedlings were then placed in a humid box, and incubated at 25°C for the first 24 h in the dark, then with a cycle of 12 h day and 12 h night. Cotyledons were collected at different time points and mounted in perfluorodecalin (Sigma Aldrich) for confocal microscopy (Littlejohn et al., 2014). Observations were made using an inverted confocal microscope (Leica SP5) equipped with a 63x water immersion objective (NA 1.2). For mCherry and mScarlet, both were excited at 561 nm and emission then detected from 600 nm to 630 nm and from 580 to 630 nm, respectively. For mNeonGreen, excitation was at 488 nm and emission was detected from 510 to 540 nm. Fluorescence images were captured in parallel with Differential Interference Contrast (DIC) transmitted light images. Line intensity profiles were generated using ImageJ.

3 | RESULTS

3.1 | EV-like structures are present in the space between the cell wall and plasma membrane in *Colletotrichum* species

Prior to the first isolation of fungal EVs, multiple studies documented the presence of fungal secreted vesicles using transmission electron microscopy. Vesicles have been observed on the cell surface of yeasts and filamentous fungi or sandwiched between the cell wall and plasma membrane, often in a state of budding from the plasma membrane or release from the cell (Anderson et al., 1990; de Paula et al., 2019; Gibson & Peberdy, 1972; Ikeda et al., 2018; Osumi, 1998; Rizzo et al., 2020; Rodrigues et al., 2007; Takeo et al., 1973; Vargas et al., 2015; Wolf et al., 2014). In some yeast species, fungal EVs were seemingly observed in the process of traversing the cell wall (Albuquerque et al., 2008; Anderson et al., 1990; Rodrigues et al., 2007).

To determine whether similar structures could be observed in species of *Colletotrichum*, we used transmission electron microscopy (TEM) to examine the biotrophic hyphae from *C. higginsianum* and *C. lindemuthianum* formed during growth inside living cells of their respective plant hosts (Figure 1). Membrane-bound vesicle-like structures were observed in the paramural space of biotrophic hyphae, between the fungal wall and plasma membrane (Figure 1a-c). These structures varied in size and shape, some appearing spherical, while others were more allantoid in shape (Figures 1b and c). However, from single ultrathin sections it is difficult to tell whether these structures represent discrete vesicles or networks of membranous tubes, similar to those produced by arbuscular mycorrhizal fungi during symbiosis (Ivanov et al., 2019; Roth et al., 2019). The irregular shapes of these structures stand in sharp contrast to the smaller, uniformly spherical intraluminal vesicles (ILVs) observed within nearby fungal multivesicular bodies (MVBs; Figure 1d). ILVs had a mean diameter of 41.9 nm (SE = 0.78, n = 71), while vesicles observed in the paramural spaces ranged from 52.0 to 363.0 nm in length and 48.2–159.2 nm in width (based on measurements of 20 structures from *C. higginsianum* and *C. lindemuthianum*). This difference in size and regularity may suggest that the extracellular structures are derived directly from the plasma membrane rather than by the fusion of MVBs with the plasma membrane. Nevertheless, these observations support the presence of EVs in *Colletotrichum* species and, if they are exported beyond the cell wall as in other fungi, it may be possible to isolate them. We also detected vesicle-like structures in the interfacial matrix between the fungal wall and plant plasma membrane (Figure 1d), but their fungal or plant origin could not be determined.

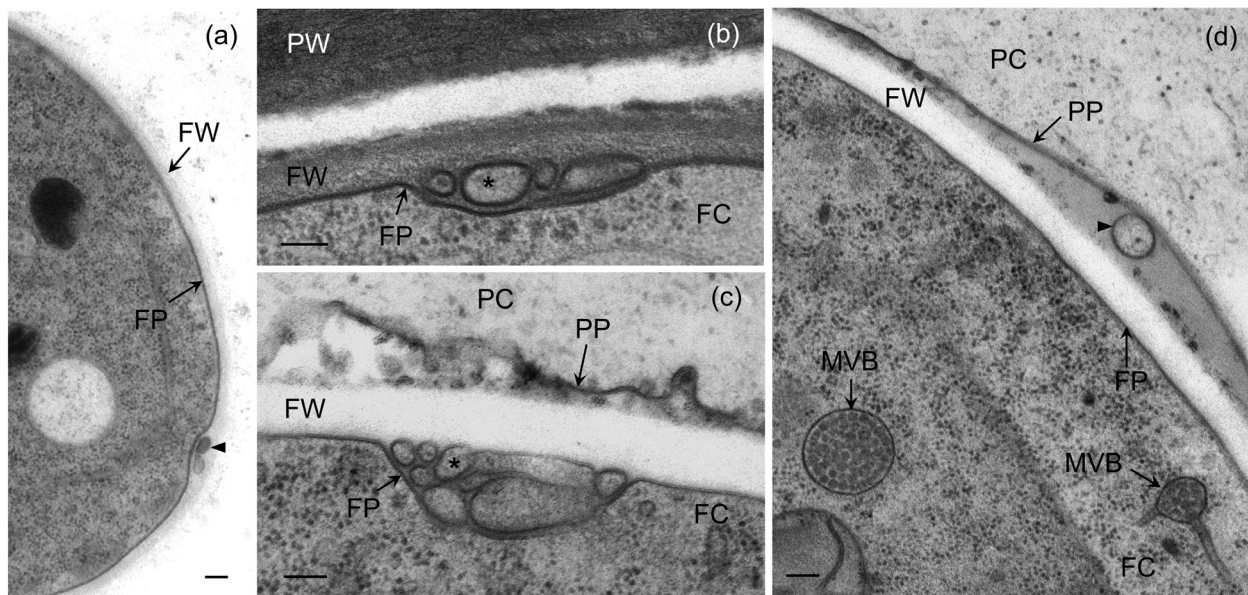


FIGURE 1 Biotrophic hyphae of *Colletotrichum higginsianum* and *C. lindemuthianum* contain extracellular vesicle-like structures in the paramural space. (a) Biotrophic hypha of *C. higginsianum* isolated from *Arabidopsis* leaves by fluorescence-activated cell sorting showing paramural vesicles (arrowhead). (b) An extracellular vesicle (arrowhead) inside the interfacial matrix layer between the fungal cell wall (FW) and the plant plasma membrane (PP). (c-d) Biotrophic hyphae of *C. lindemuthianum* infecting *Phaseolus vulgaris* epidermal cells. (c, d) Paramural vesicles (asterisks) between the fungal cell wall (FW) and fungal plasma membrane (FP). All cells were prepared for TEM by high-pressure freezing and freeze-substitution. FC, fungal cytoplasm; MVB, multivesicular body; PC, plant cytoplasm; PW, plant cell wall. Scale bars = 100 nm

3.2 | EV-like particles can be isolated from the supernatant of *C. higginsianum* protoplasts

Fungal EVs were first isolated from the supernatants of *Cryptococcus neoformans* liquid cultures (Rodrigues et al., 2007). This approach has since been used to study EVs in multiple species of yeasts and filamentous fungi, including phytopathogens (Kwon et al., 2021; Rizzo et al., 2020). As a first attempt to isolate EVs from *C. higginsianum*, we processed the supernatant of 3-day-old liquid cultures using differential ultracentrifugation. To our surprise, despite processing relatively large volumes of supernatant and using high speeds, we were unable to detect meaningful numbers of EV-like particles. Nano-particle tracking analysis (NTA) failed to identify high numbers of particles in the final pellet (Figure 3 and Figure S1) and while TEM negative staining did reveal some cup-shaped objects reminiscent of vesicles, such structures were rare (Figure S1).

One explanation for the scarcity of EVs in our culture supernatants could be that *C. higginsianum* only releases EVs under specific circumstances, which we were unable to recreate in the medium tested (Mathur's medium). Another possibility is that *C. higginsianum* EVs were produced, but the majority remained trapped between the fungal cell wall and plasma membrane. To determine if the cell wall blocked the release of EVs into the liquid culture, we generated *C. higginsianum* protoplasts using a mixture of fungal cell wall-degrading enzymes. Supernatants obtained from protoplast digestion reactions were filtered and processed using differential ultracentrifugation. The resulting crude pellet was then purified on a discontinuous Optiprep gradient.

We selected six fractions from the middle of the density gradient ranging from 10 - 40% Optiprep (Figure 2a). From our experience with plant EVs, we expect vesicles to float somewhere in this region (Rutter & Innes, 2017). Using NTA, we observed the highest concentrations of particles in fractions three, five and six with corresponding densities of ~ 1.078 , ~ 1.115 and ~ 1.173 g/ml (Figure 2b). Particles in these fractions had an average diameter of ~ 106 , ~ 102 and ~ 100 nm, respectively (Figure 2c). The median diameters for fractions three, five and six were ~ 104 , ~ 102 and ~ 100 nm, respectively. Negative staining and TEM analysis revealed abundant, cup-shaped structures in all three fractions (Figure 2d). The size and morphology of the particles in these fractions, as well as their ability to float, suggest they are lipid vesicles. Furthermore, it appears that two separate populations of vesicles were released into the supernatant, a low density (LD) population in fraction three and a high density (HD) population in fractions five and six.

To demonstrate further that generating protoplasts is key to the isolation of EV-like particles from *C. higginsianum*, we processed the supernatants of undigested mycelia and protoplasts in parallel. Both fungal samples were derived from an equal mass of mycelia and were treated under the same conditions, except that one was incubated in a buffer containing hydrolyzing enzymes and the other was incubated in a buffer lacking enzymes. After differential ultracentrifugation and purification on a density gradient, we detected significantly higher concentrations of particles in fractions isolated from the supernatant of protoplasts compared to those isolated from the supernatant of undigested mycelia (Figure 3). The results show that significant numbers

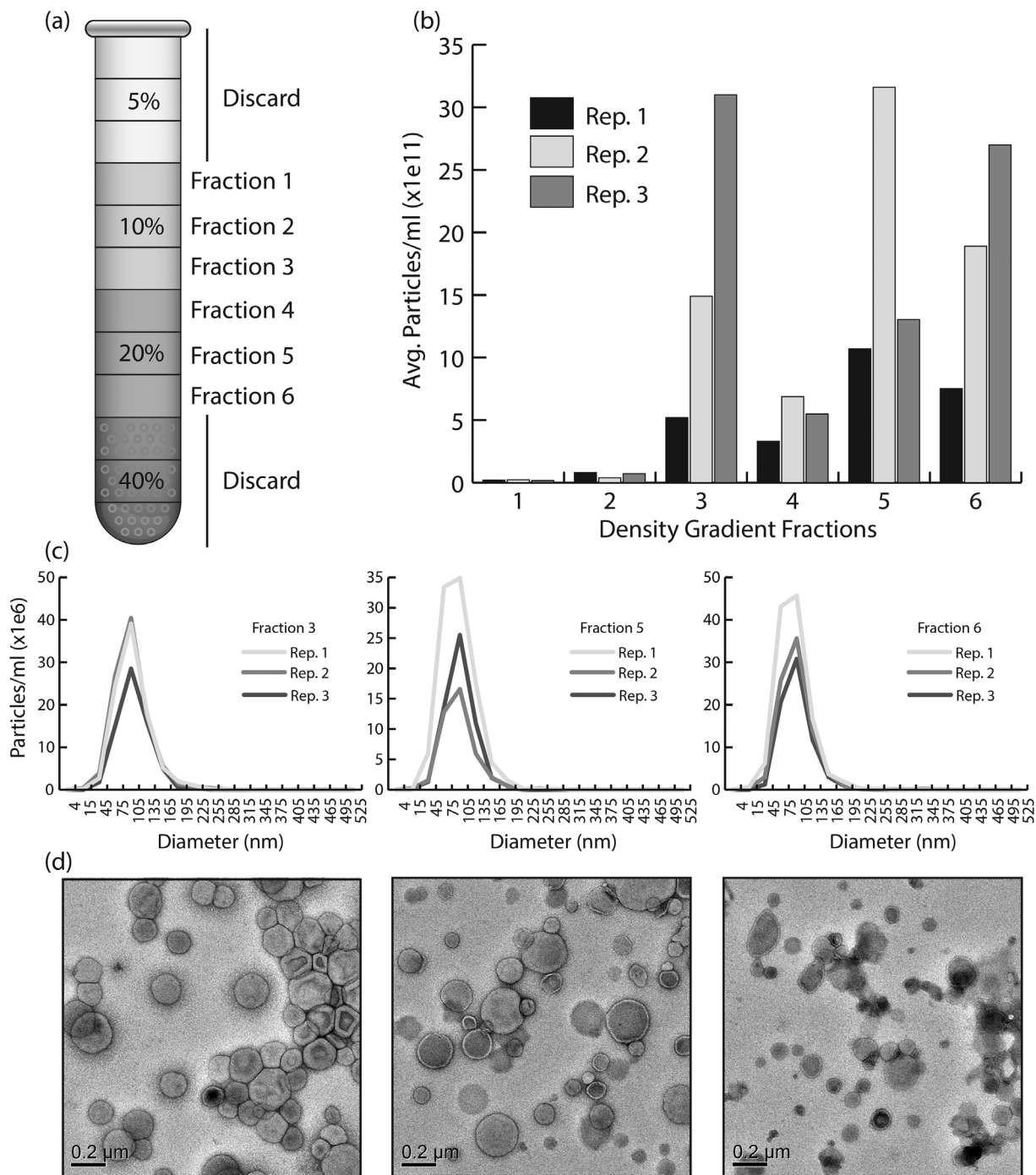


FIGURE 2 Vesicle-like structures can be purified from *C. higginsianum* protoplasts. (a) Schematic of the Optiprep gradient used to purify vesicles. Crude vesicle pellets were bottom-loaded into a discontinuous Optiprep gradient consisting of 5, 10, 20 and 40% layers. After centrifugation at 100K x g for 17 h, the 5% layer was discarded and the next six fractions of 1 ml each were collected and processed with further ultracentrifugation to obtain a pure vesicle pellet. (b) Nanoparticle tracking (NTA) data showing the average concentration of particles in each of the collected Optiprep fractions. Three independent experiments are shown in one graph. (c) NTA data showing the size distribution of particles in fractions 3, 5 and 6. Three replicates are shown in each line graph. (d) Transmission electron microscopy negative stain images of fractions 3, 5 and 6

of EV-like particles are only released into the supernatant after the removal of the fungal cell wall. These results also help allay concerns about hyphal tip bursting. Mechanical agitation, as well as changes in osmotic and temperature conditions during the formation of protoplasts can cause the spontaneous bursting of hyphal tips (Bartnicki-Garcia & Lippman, 1972). Such damage would lead to a discharge of intracellular components into the supernatant, which could become confounding artifacts. Our results, however, suggest that if any hyphal tip rupture does occur, it does not generate a significant number of particles. We also assessed the viability of the protoplasts to determine if broken protoplasts might contribute to particle release. Using Evans blue,

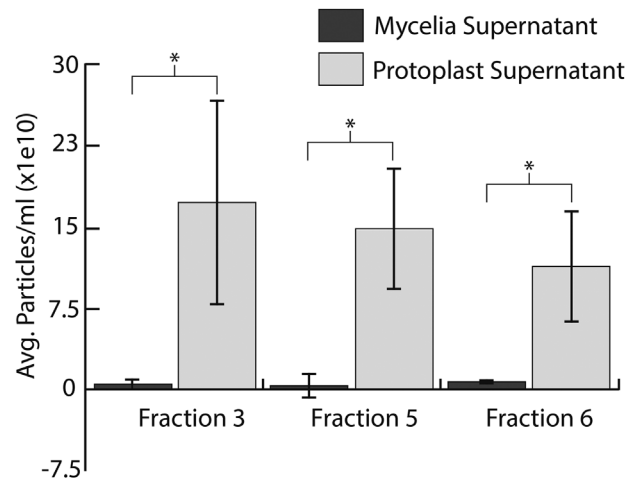


FIGURE 3 Isolating particles from *C. higginsianum* protoplasts requires removal of the cell wall. Supernatant from mycelia in a mock digest solution or protoplasts were processed in parallel to purify vesicles. Significant numbers of particles were only detected in samples from protoplasts. Bars represent an average of three independent experiments. Error bars represent SD. Asterisks signify a significant difference based on a two-tailed unpaired Student's *t* test ($P < 0.05$)

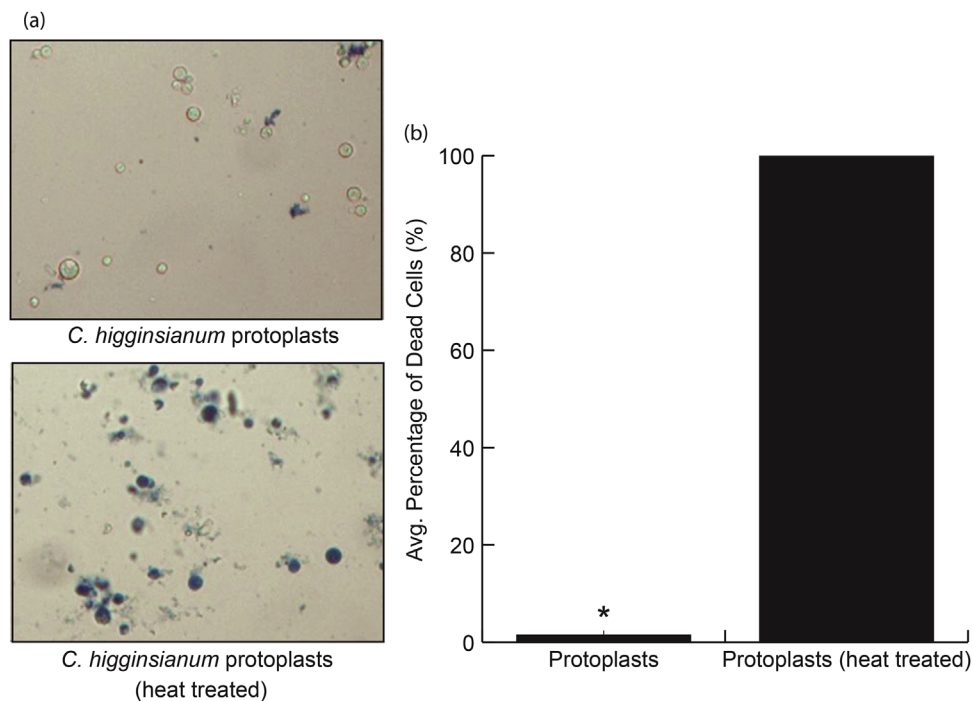


FIGURE 4 Viability stain of *C. higginsianum* protoplasts. (a) Protoplasts generated after cell wall digestion were mixed with Evans blue dye to a final concentration of 0.04% and observed for staining using a light microscope. A sample of protoplasts was incubated at 95 °C for 5 min and mixed with dye to provide a positive control for staining. (b) 300 protoplasts were tallied for untreated and heat-treated. The graph represents the mean number of dead protoplasts from three independent experiments. Error bars represent SD. The asterisk signifies the value is significantly different from the other based on a two-tailed unpaired Student's *t* test ($P < 1e-8$)

an exclusion dye that labels cells with damaged plasma membranes (Gaff & Okong'O-Ogola, 1971), we found that the percentage of nonviable protoplasts produced after cell wall digestion was ~1.6% (Figures 4a and b). The overwhelming majority of protoplasts (98.4%) remained viable after cell wall digestion, suggesting that the EV-like particles are not derived from damaged protoplasts (Figure 4b). However, we cannot exclude the possibility that intercellular or artefactual vesicles were released during the formation of protoplasts.

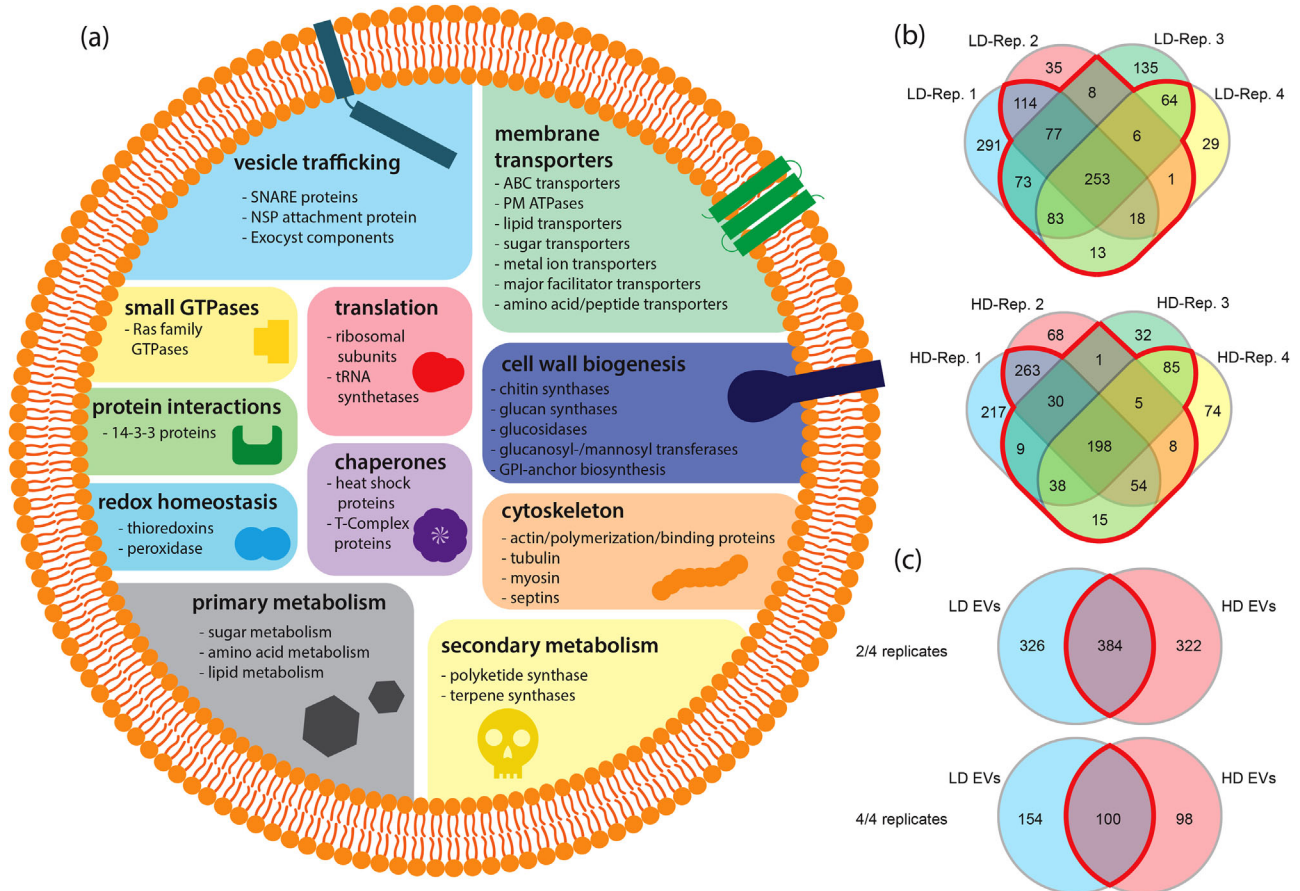


FIGURE 5 Overview of the *C. higginsianum* EV Proteome. (a) Overview of categories of proteins found in both low density (LD) and high density (HD) vesicles purified from *C. higginsianum* protoplasts. (b) Venn diagrams showing the overlap of proteins detected by mass spectrometry between independent replicates of purified LD and HD vesicles (proteomes selected were present in two out of four replicates, q-value ≤ 0.01). The red outlined region contains proteins shared by at least two replicates. (c) Venn diagrams showing the overlap between the LD and HD vesicle proteomes. The red outlined region is shared. When the proteomes selected were present in two out of four replicates with a q-value ≤ 0.01 , approximately 46% of proteins in each population of vesicles were shared. When stricter criteria were applied (i.e., four out of four replicates, q-value ≤ 0.01), approximately 40% of LD and 60% of HD proteins were held in common

3.3 | The protein content of *C. higginsianum* EV-like particles

Having purified two populations of *C. higginsianum* vesicles, we next sought to analyse the proteins associated with each population. Crude vesicle samples were treated with trypsin to remove extravascular proteins. The samples were then purified on a density gradient to separate low- and high-density populations and analysed using LC-MS/MS (Table S1). We selected proteins detected in two out of four replicates with a q-value ≤ 0.01 . After applying these criteria, we generated a list of 710 proteins associated with the low-density (LD) vesicles and 706 proteins associated with the high density (HD) vesicles (Table S2). Approximately 59% of proteins were common to at least two LD replicates and $\sim 64\%$ were common to at least two HD replicates (Figure 5b). The LD and HD populations shared 384 proteins ($\sim 54\%$ of both LD and HD proteins), while 326 were unique to the LD population and 322 were unique to the HD population (Figure 5c). Applying the strictest criteria, analysing only the proteins with a q-value ≤ 0.01 found in all four replicates, reduced the number of proteins in the LD population to 253 and the number of proteins in the HD population to 198. One hundred of these proteins ($\sim 40\%$ of LD proteins and $\sim 60\%$ of HD proteins) were common between the two populations (Figure 5c).

Mammalian EVs are associated with a common set of proteins that include transmembrane proteins (annexins and tetraspanins), vesicle trafficking proteins (ESCRT proteins and Rab GTPases), cytoskeletal proteins, heat-shock proteins, metabolic enzymes, integrins, 14-3-3 proteins and ribosomal subunits (Choi et al., 2015). Fungal EVs contain many similar proteins and are often enriched for proteins that function in the plasma membrane, cell wall biogenesis, pathogenesis, stress responses, transport, signalling and basic cellular metabolism (Bleackley et al., 2019). Between the two populations of vesicles from *C. higginsianum*, we identified several proteins commonly associated with EVs in both mammals and fungi. GO term enrichment was determined using FungiFun2 (Priebe et al., 2015). The most enriched EV proteins in both fractions were membrane transporters (e.g., ABC and MFS transporters, plasma membrane proton ATPases), small GTPases, enzymes involved in

amino acid and carbohydrate metabolism, as well as proteins involved in vesicle-mediated transport and translation (ribosomal subunits) (Figure 5a, Tables S1, S2). We also detected other classes of proteins involved in cytoskeleton organization, protein folding (heat-shock proteins), cell redox homeostasis and the synthesis of secondary metabolites (Figure 5a, Tables S1–S3). While the majority of proteins were shared between the LD and HD fractions, the LD population was enriched for GO terms related to translation, amino acid metabolism, intercellular transport and actin filament polymerization (Table S4). The HD population was enriched for GO terms related to protein and lipid metabolism, protein folding and exocytosis, as well as membrane anchoring and docking (Table S4).

Extracellular vesicles are commonly associated with plasma membrane proteins (Bleackley et al., 2019). We found that approximately 19.7% and 35.4% of LD and HD vesicle proteins, respectively, had predicted transmembrane regions (Table S2). Membrane proteins associated with the vesicles included those involved in SNARE complexes (v-SNARES, t-SNARES and NSF attachment proteins), transport across membranes (ABC and MFS transporters, proton ATPases, sugar transporters, amino acid transporters, peptide transporters, lipid transporters) or recruitment of proteins to membranes (PH domain containing proteins, C2 domain proteins; Tables S1, S2). The vesicle proteomes also contained multiple GTPases (Ras, Rab, Ran and Rho GTPases) that function to regulate vesicle trafficking (Tables S1, S2). Interestingly, homologs of the *C. higginsianum* t-SNARE Sso2 (OBR10381) as well as the GTPases Ced-10 (OBR05828), RhoA (OBR05976), Rab-8A (OBR12345) Rab-11B (OBR03559), Arf3 (OBR07035) and Cell Division Control Protein 42 (OBR14052) were recently identified as EV markers in *C. albicans* (Dawson et al., 2020). These SNARES and GTPases were all present in the *C. higginsianum* LD and HD vesicle populations and could represent conserved fungal EV markers (Tables S1, S2).

A recent study attempting to define protein markers for *Candida albicans* EVs proposed 22 different proteins that were enriched in EVs compared to the whole cell lysate. The list includes three Sur7 proteins, which are four transmembrane domain proteins localized in plasma membrane subdomains known as eisosomes in yeasts and filamentous fungi (Dawson et al., 2020). Interestingly, Sur7 proteins were also identified in EVs from the genus *Cryptococcus* and the wheat pathogen *Zymoseptoria tritici* (Hill & Solomon, 2020; Rizzo et al., 2021). Surprisingly, while we did detect Sur7-like proteins (OBR09999, OBR07542, OBR09056), they were not present at high enough peptide counts or in enough replicates to meet our criteria (Table S1). This suggests that, unlike *C. albicans* and members of the genus *Cryptococcus*, Sur7 proteins may not be enriched in *C. higginsianum* EVs. However, it should be noted that because our EV samples were pretreated with trypsin, regions of Sur7 proteins on the surface of vesicles would have been degraded, making these proteins more difficult to detect by LC-MS/MS. For the same reason, it is possible that the calculated overall percentage of transmembrane proteins identified in both vesicle populations may have been underestimated.

Fungal EVs are often associated with enzymes thought to function in cell wall synthesis and remodelling (Oliveira et al., 2010; Rizzo et al., 2020; Zhao et al., 2019). EVs from *S. cerevisiae* have the ability to promote cell wall remodelling in mutants with wall defects (Zhao et al., 2019), while EVs secreted from protoplasts of *A. fumigatus* are associated with fibrillar material and cell wall regeneration (Rizzo et al., 2020). EVs from *C. neoformans* were also observed passing through the cell wall, a process suggested to be made possible by enzyme-mediated cell wall remodelling (Wolf et al., 2014). Among LD and HD vesicle populations from *C. higginsianum*, we detected a total of twenty enzymes likely to be involved in remodelling of the fungal cell wall, including the synthesis or degradation of chitin (6), alpha-1,3-glucans (3) and beta-1,3-glucans (11) (Tables S1 and S2). The presence of these proteins suggests a role for *C. higginsianum* EVs in cell wall biology.

We also detected proteins associated with the production of secondary metabolites (Table S3). Species of *Colletotrichum* as well as other pathogenic fungi produce secondary metabolites, including polyketides, nonribosomal peptides, alkaloids and terpenes. These metabolites often serve important roles in pathogenicity or virulence (Pusztahelyi et al., 2015). HD vesicles were associated with proteins encoded by Biosynthetic Gene Cluster 16 (BGC16), which is involved in the production of higginsianin A to E. These metabolites are diterpenoid α -pyrones that have cytostatic and cytotoxic activities in mammalian cancer cells (Cimmino et al., 2016; Sangermano et al., 2019). In plants, higginsianin B inhibits the activation of jasmonate (JA) defense signalling by exogenous JAs, as well as the wound-induced activation of this pathway (Dallery et al., 2020). Proteins involved in the higginsianin biosynthetic pathway present in the HD vesicle population included flavin-containing superfamily amine oxidase (OBR09790), terpene cyclase (OBR09784) and prenyltransferase (OBR09786; Table S3). Four other proteins in the pathway (geranylgeranyl pyrophosphate synthase (OBR09788), FAD-dependent epoxidase (OBR09783) and short-chain dehydrogenases (OBR09785 and OBR09787)) were also detected but did not meet our criteria for inclusion in the final proteome (Table S1).

Proteins encoded by two additional secondary metabolite BGCs (BGC21 and BGC71) were also detected in LD and HD vesicles (Table S3). BGC21 comprises 12 genes encoding OBR10834 to OBR10845, including a polyketide synthase (PKS, OBR10843) and a terpene cyclase (OBR10835). This BGC is absent from other sequenced *Colletotrichum* spp. but homologs occur in diverse phylogenetically distant fungi (Figures S2a and S2b). No characterized chemical product has been described for any of the homologous BGCs, suggesting that BGC21 produces an unknown family of molecules (Table S5). BGC71 comprises 11 genes encoding OBR03047 to OBR03057 and is conserved in most *Colletotrichum* spp. and several Dothideomycetes, all of which are plant pathogens (Figures S3a and S3b). OBR03057 was detected in both LD and HD vesicles and together with OBR03051 and OBR03052, these three proteins resemble the lovastatin/monacolin BGC (Table S6). BGC71 may thus produce lovastatin-like molecules that could contribute to fungal pathogenicity.

Transcriptomic data from *C. higginsianum* grown *in planta* or *in vitro* suggest that BGC16 and 21 are both transcriptionally induced during the biotrophic and necrotrophic stages of infection. This suggests that the products of these BGCs are linked to pathogenicity and could be exported in EVs during infection as well as axenic growth. BGC71, however, does not show a clear pattern of expression linked to the examined developmental or infection stages (Table S3, Figure S4).

Finally, we used SignalP-5.0 to predict the number of vesicle-associated proteins with N-terminal signal peptides (SPs). As an unconventional pathway for secretion, EVs usually have a lower percentage of proteins with SPs. For example, only 6.7% of EV proteins from the wheat pathogen *Zymoseptoria tritici* had a predicted SP (Hill & Solomon, 2020), while 12.5–22% of EV proteins from the cotton pathogen *Fusarium oxysporum* f. sp. *vasinfectum* had a predicted SP, depending on the medium in which the fungus was grown (Bleackley et al., 2019; Garcia-Ceron et al., 2021). Compared to these other filamentous plant pathogens, 4.9% of *C. higginsianum* LD vesicle proteins and 16.4% of HD vesicle proteins have a predicted signal peptide (Table S2).

3.4 | Development of transgenic EV marker strains

Biomarkers are crucial tools in EV research; they can aid the identification, authentication, tracking and purification of vesicles. In an effort to establish general protein biomarkers for *C. higginsianum* EVs, we selected protein candidates common to both the LD and HD populations that would serve as markers for vesicle membrane or luminal cargo. To mark the vesicle membrane, we selected the v-SNARE *ChSnc1* (OBR08408) and the t-SNARE *ChSso2* (OBR10381), which are both integral membrane proteins and members of the Snc1/2, Sso1/2, Sec9 SNARE complex. All members of this complex are present in the EV proteome. SNARE proteins are highly conserved across species, often maintaining the same function at different membrane trafficking steps (Bock et al., 2001; Gupta & Brent Heath, 2002; Kloepper et al., 2007). The Snc1/2, Sso1/2, Sec9 SNARE complex functions in the docking and fusion of exocytic vesicles with the plasma membrane (Aalto et al., 1993; Brennwald et al., 1994; Rossi et al., 1997). Orthologous SNARE proteins in other species of fungi have important roles in pathogenesis. For example, orthologs of *ChSso2* mediate the secretion of pathogenesis-related degradation enzymes in *C. albicans* and the unconventional secretion of effectors in the phytopathogens *M. oryzae* and *V. dahliae* (Bernardo et al., 2014; Giraldo et al., 2013; Wang et al., 2018) and trichothecene phytotoxins in *Fusarium graminearum* (O'Mara et al., 2020). Moreover, orthologs of Snc1/2, Sso1/2 or Sec9 have been identified in the EV proteomes of *S. cerevisiae*, *C. albicans*, *A. fumigatus* and *C. neoformans* (Dawson et al., 2020; Rizzo et al., 2020; Wolf et al., 2014; Zhao et al., 2019).

As a marker for EV luminal cargo, we selected the 14-3-3 protein *ChBmh1* (OBR15609), one of two such proteins we detected in LD and HD vesicles. Members of the 14-3-3 family mediate protein-protein interactions and are involved in a myriad of cellular process, including cell division, vesicle trafficking, stress responses, signalling and apoptosis (Gelperin et al., 1995; Kumar, 2017; Roth et al., 1999; van Heusden & Steensma, 2006). 14-3-3 proteins are common in mammalian EVs (Choi et al., 2015), and have also been identified in the EV proteomes of several fungi, including *C. neoformans*, *S. cerevisiae*, *F. oxysporum* f. sp. *vasinfectum*, *C. albicans*, *Z. tritici* and *A. fumigatus*, all of which possess at least one ortholog of *ChBmh1* (Bleackley et al., 2019; Dawson et al., 2020; Hill & Solomon, 2020; Rizzo et al., 2020; Wolf et al., 2014; Zhao et al., 2019).

To test the association of our selected markers with *C. higginsianum* EVs and to validate our proteomic data, we generated transgenic strains expressing fluorescent-tagged marker proteins. *ChSnc1* and *ChSso2* were expressed as N-terminal fusions with mScarlet and mNeonGreen, respectively, while *ChBmh1* was expressed as a C-terminal fusion with mCherry. The mScarlet-*ChSnc1* construct was expressed from the native promoter, while the two others were placed under control of the *ChActin* promoter because their fluorescence signals were too weak or not detectable using their respective native promoters. The expression of each fluorescent fusion protein was verified in axenic mycelial cultures using confocal microscopy.

The mScarlet-*ChSnc1* fusion protein appeared to localize to the fungal plasma membrane and to small, mobile puncta that were concentrated near the hyphal apex (Figure 6a). Some hyphae also showed a small focal accumulation beneath the plasma membrane at the hyphal apex (Figure 6b), which likely corresponds to the Spitzenkörper (SPK), a cluster of microfilaments and vesicles that is pivotal for polar growth and apical secretion in fungi (Riquelme & Sanchez-Leon, 2014). Concentration of Snc1 in the SPK was previously reported in *Trichoderma reesei* (Valkonen et al., 2007). In older, subapical regions, mScarlet-*ChSnc1* labelled septa, PM and vacuoles (Figure 6c). A similar localization of Snc1 proteins was reported in hyphae of *Fusarium graminearum* (Zheng et al., 2018), *Magnaporthe oryzae* (Giraldo et al., 2013) and *Aspergillus oryzae* (Hayakawa et al., 2011; Kuratsu et al., 2007). The mNeonGreen-*ChSso2* fusion protein predominantly labelled septa and the plasma membrane in older, septate hyphal compartments, whereas fluorescence intensity appeared lower in the apices of young hyphae and lateral branch hyphae (Figures 6d and e, Figure S6a). Finally, *ChBmh1*-mCherry appeared uniformly distributed through the cytoplasm of hyphae but was excluded from vacuoles (Figure 6g). In some hyphal apices, a small focal accumulation of *ChBmh1*-mCherry was also detected (Figure 6f, Figure S6b), which may correspond to the SPK.

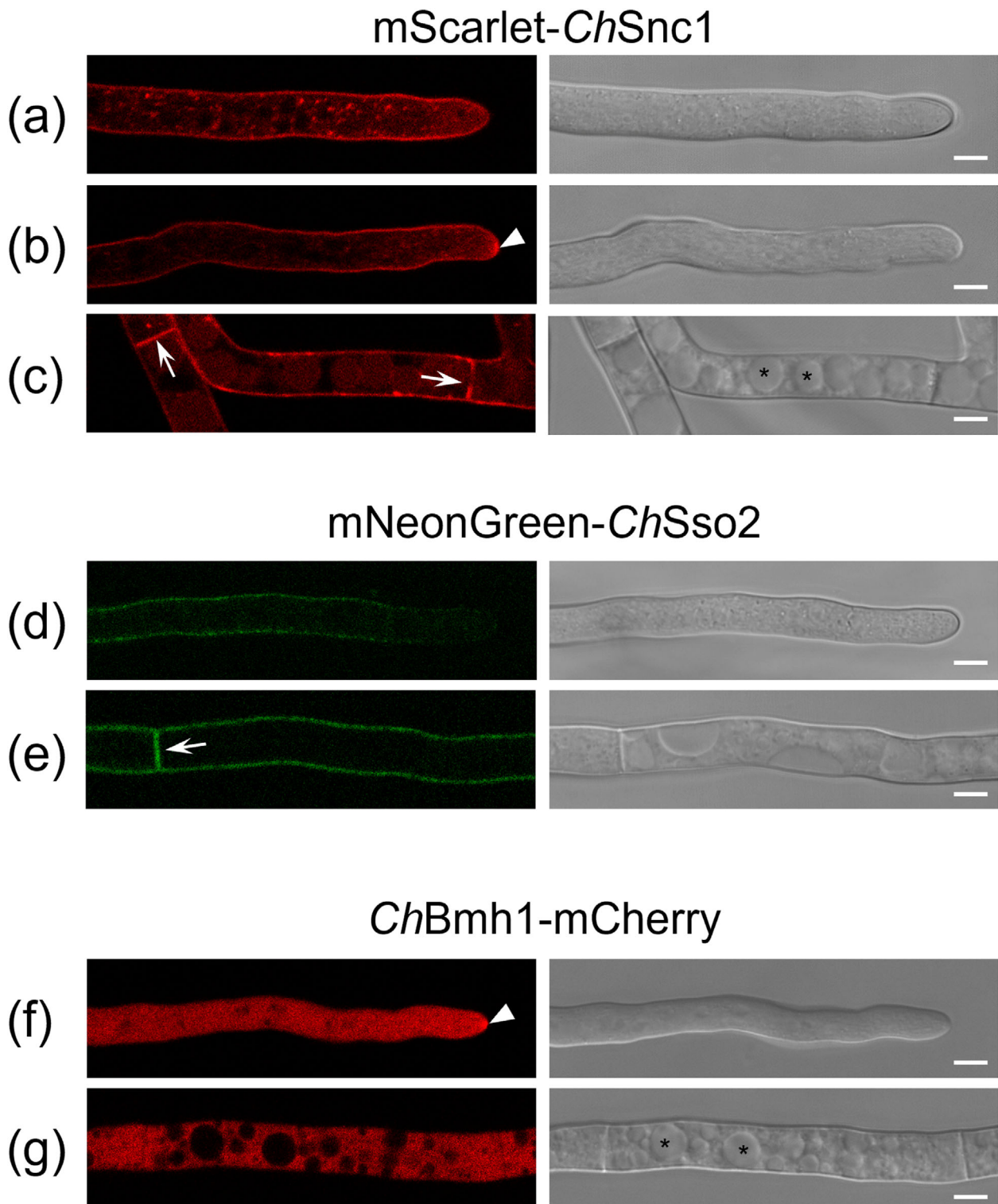


FIGURE 6 Localization of EV marker proteins in vegetative hyphae on Mathur's agar. Confocal laser scanning microscope images showing fluorescence and DIC channels. mScarlet-*ChSnc1* appeared to localize to the fungal plasma membrane (PM) and small, mobile punctae concentrated near the hyphal apex (a), as well as the Spitzenkörper (SPK, arrowhead) (b). In older, subapical regions, mScarlet-*ChSnc1* labelled septa (arrows), the PM and vacuoles (asterisks) (c). mNeonGreen-*ChSso2* labelled septa (arrow) and the PM in older subapical regions (e), with fluorescence intensity progressively decreasing toward the hyphal tip (d). *ChBmh1*-mCherry was distributed throughout the hyphal cytoplasm but was excluded from vacuoles (f, g, asterisks) and in some hyphae the SPK (arrowhead) was strongly labelled (f). Scale bars = 5 μ m

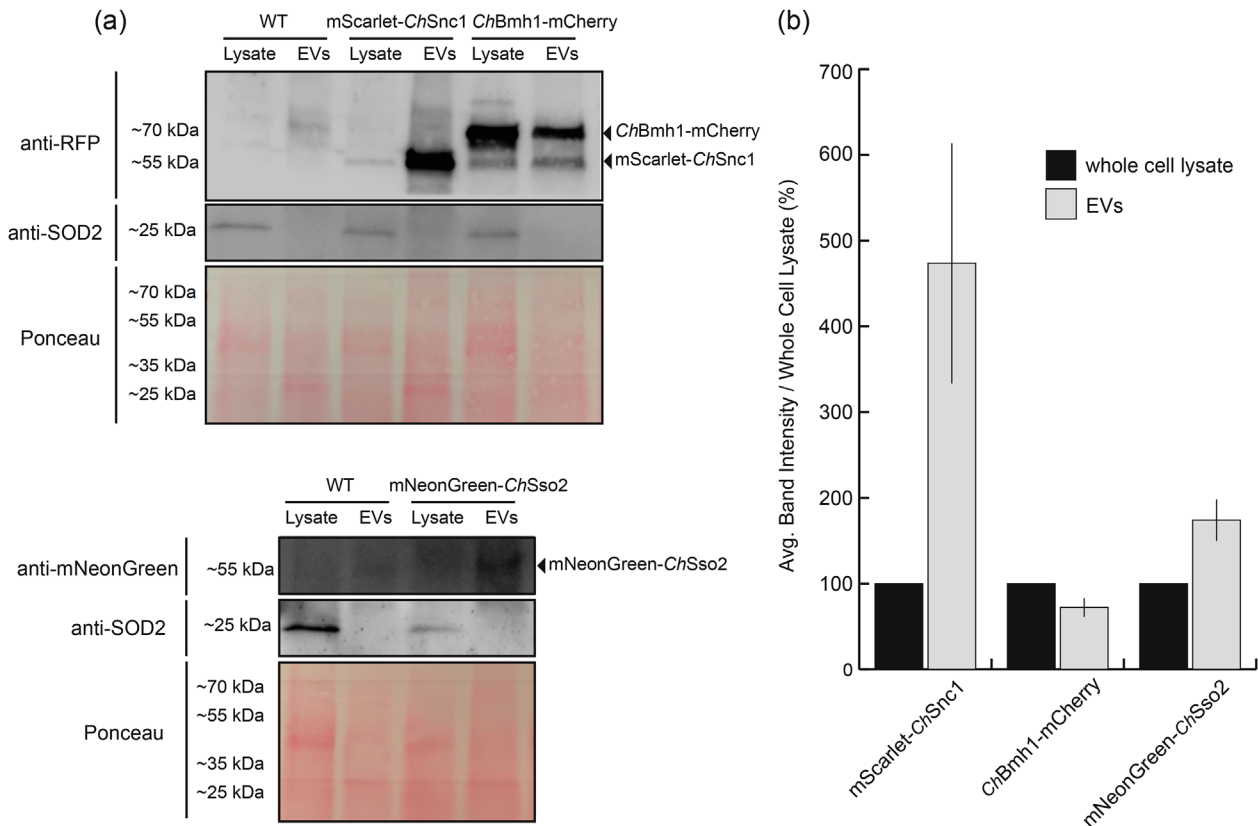


FIGURE 7 Detection of transgenic markers in EV samples. (a) Crude vesicle pellets from transgenic marker strains and nontransgenic wild-type fungi were isolated and probed for the fluorescent-tagged proteins RFP or mNeonGreen by immunoblot. EV markers were detected in samples of protoplast lysate as well as crude vesicle samples, while the contamination marker SOD2 was only detected in the sample of mycelial lysate. (b) EV marker band intensities were quantified and expressed as a percentage of the band intensity for the whole cell lysate. Bars represent the average of two independent replicates

3.5 | Fluorescent EV marker proteins are protected inside EVs

To validate the association of our selected marker proteins with *C. higginsianum* EVs, we grew mycelial cultures of each transgenic strain alongside wild type, nontransgenic *C. higginsianum*. Protoplasts were generated from each culture, and crude EV samples were isolated from the supernatant. Equal amounts of protein from samples of whole-cell lysate and EVs were probed for fluorescent-tagged proteins using an immunoblot. We detected mScarlet-*ChSnc1*, *ChBmh1-mCherry* and mNeonGreen-*ChSso2* by immunoblot in lysate and vesicle samples from transgenic fungi but not in samples from the nontransgenic fungus (Figure 7). Both mScarlet-*ChSnc1* and mNeonGreen-*ChSso2* appeared to be enriched in EV samples compared to whole-cell lysate. It makes sense that both SNARE proteins would be enriched, because they interact in the same complex. However, the signal for mNeonGreen-*ChSso2* was much weaker than that of mScarlet-*ChSnc1*. This lower level of expression could be a result of the mNeonGreen tag, which was not codon optimized for this fungus. We also probed vesicle samples for native Superoxide Dismutase 2 (SOD2), a mitochondrial protein that was recently identified as a potential negative EV marker (Dawson et al., 2020). While we detected SOD2 in samples of mycelial lysate, we were unable to detect it in vesicle samples from transgenic or nontransgenic fungi (Figure 7). These results show that vesicle samples are enriched for our selected EV markers but not a marker for contamination, indicating that these vesicles are unlikely to be the product of cell lysis.

Finally, we wanted to confirm that our fluorescent marker proteins were present inside fungal EVs rather than merely copelleting with the vesicles. To do this, we subjected vesicle samples to a protease protection assay. Vesicle samples were treated with either buffer, trypsin or detergent followed by trypsin. Proteins protected inside of vesicles are expected to remain intact after trypsin treatment unless detergent has been added to solubilize lipid membranes. Again, our marker proteins were detected in the lysate of transgenic mycelia and in crude vesicle samples. Importantly, the proteins were still detected in vesicle samples after treatment with trypsin but could not be detected when the samples were pretreated with detergent followed by trypsin (Figure 8). These results indicate that the marker fusion proteins are packaged inside of fungal EVs, where they are protected from degradation. This helps validate our proteomic data and suggests that *ChSnc1*, *ChSso2* and *ChBmh1* can all function as markers for *C. higginsianum* EVs. However, mNeonGreen-*ChSso2* may require additional optimization to be reliably detected in fungal mycelia and EVs.

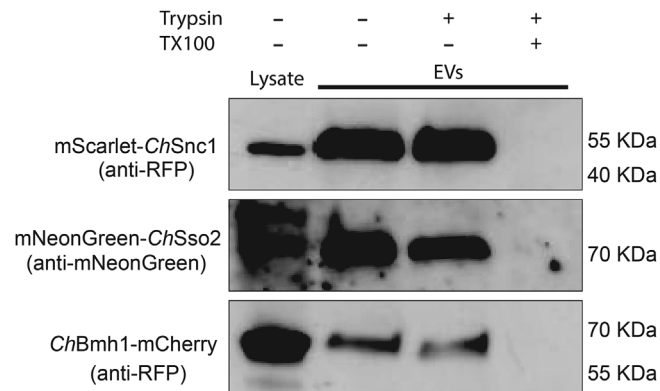


FIGURE 8 Transgenic EV markers are protected inside of lipid vesicles. A sample of crude vesicles from each EV marker strain was split into three and either left untreated, treated with trypsin or treated with detergent followed by trypsin. EV markers were then detected by immunoblot. Detection of the fusion protein in the presence of trypsin but not in the presence of detergent plus trypsin indicates the protein is protected within a lipid compartment. All experiments were repeated twice

3.6 | Localization of EV markers during infection

One of the reasons for developing the above EV marker strains was to enable tracking of EVs during infection of plants. To this end, we infected *Arabidopsis* leaves with our transgenic EV marker strains and observed the localization of each marker at different stages of development. Early in infection, the *C. higginsianum* spore germinates and produces a nascent, prepenetration appressorium devoid of melanin. Over time, the appressorium matures and its cell wall becomes melanized. The base of this specialized structure contains a penetration pore from which a needle-like penetration peg emerges to pierce the cuticle and plant cell wall. After the fungus successfully penetrates the plant cell wall, it produces a bulbous, multilobed biotrophic hypha. Eventually, the fungus transitions to a necrotrophic stage, producing long, thin necrotrophic hyphae capable of invading and overwhelming neighbouring cells (O'Connell et al., 2004). We examined the localization of markers in spores, appressoria, biotrophic hyphae and necrotrophic hyphae.

In spores expressing mScarlet-*ChSnc1*, we observed numerous punctate bodies that were possibly small vacuoles (Figure S5). In appressoria, mScarlet-*ChSnc1* signals were also observed in small fluorescent puncta arranged around the cell periphery (Figures 9a and 9b), and in some young appressoria the plasma membrane was also weakly labelled (Figure S5). Within young biotrophic hyphae, mScarlet-*ChSnc1* was uniformly distributed in the plasma membrane and in small puncta (Figures 9c and 9d), whereas in more mature biotrophic hyphae the plasma membrane labelling was more concentrated at hyphal tips (Figures 9e and 9f). After the transition to necrotrophy, mScarlet-*ChSnc1* similarly appeared to localize to the apical plasma membrane of necrotrophic hyphae, and numerous vacuoles of varying sizes were also intensely labelled (Figures 9g to 9j). The fluorescent signal for mNeonGreen-*ChSso2* was relatively weak, even when expressed from the actin promoter, and no signals were detectable in either spores or appressoria. However, in biotrophic hyphae, mNeonGreen-*ChSso2* appeared to localize to the plasma membrane as well as to septa (Figures 10c and 10d). Labelling of the plasma membrane with mNeonGreen-*ChSso2* appeared weaker in necrotrophic hyphae compared to biotrophic hyphae (Figures 10a and 10b). Similar to mScarlet-*ChSnc1*, *ChBmh1*-mCherry localized to small punctate bodies in spores (Figure S5), appressoria (Figures 11a and 11b), and young biotrophic hyphae (Figures 11c to 11f). However, the fusion protein showed a strikingly different localization in more mature biotrophic hyphae (Figures 11g and 11h) and necrotrophic hyphae (Figures 11i and 11j), where *ChBmh1*-mCherry was instead distributed throughout the cytoplasm, but excluded from vacuoles.

At no point during the infections were we able to observe potential extracellular signals for our EV markers, neither in the plant apoplast nor inside the plant cytoplasm. Capturing such signals may require more sensitive imaging techniques or sampling at other timepoints. However, mScarlet-*ChSnc1* was consistently concentrated at hyphal apices, which are regions of intense polarized secretion (Riquelme & Sanchez-Leon, 2014). Whether the localization of mScarlet-*ChSnc1* to this region implies EV release occurs at hyphal tips or only the presence of abundant secretory vesicles remains to be determined.

4 | DISCUSSION

Fungal plant pathogens rely on large secretomes to successfully infect plants (Krijger et al., 2014). While much of the fungal secretome is released through conventional mechanisms, a large percentage of proteins secreted by fungal phytopathogens can exit the cell through unconventional pathways (Giraldo et al., 2013; Kim et al., 2013; Nogueira-Lopez et al., 2018; Wang et al.,

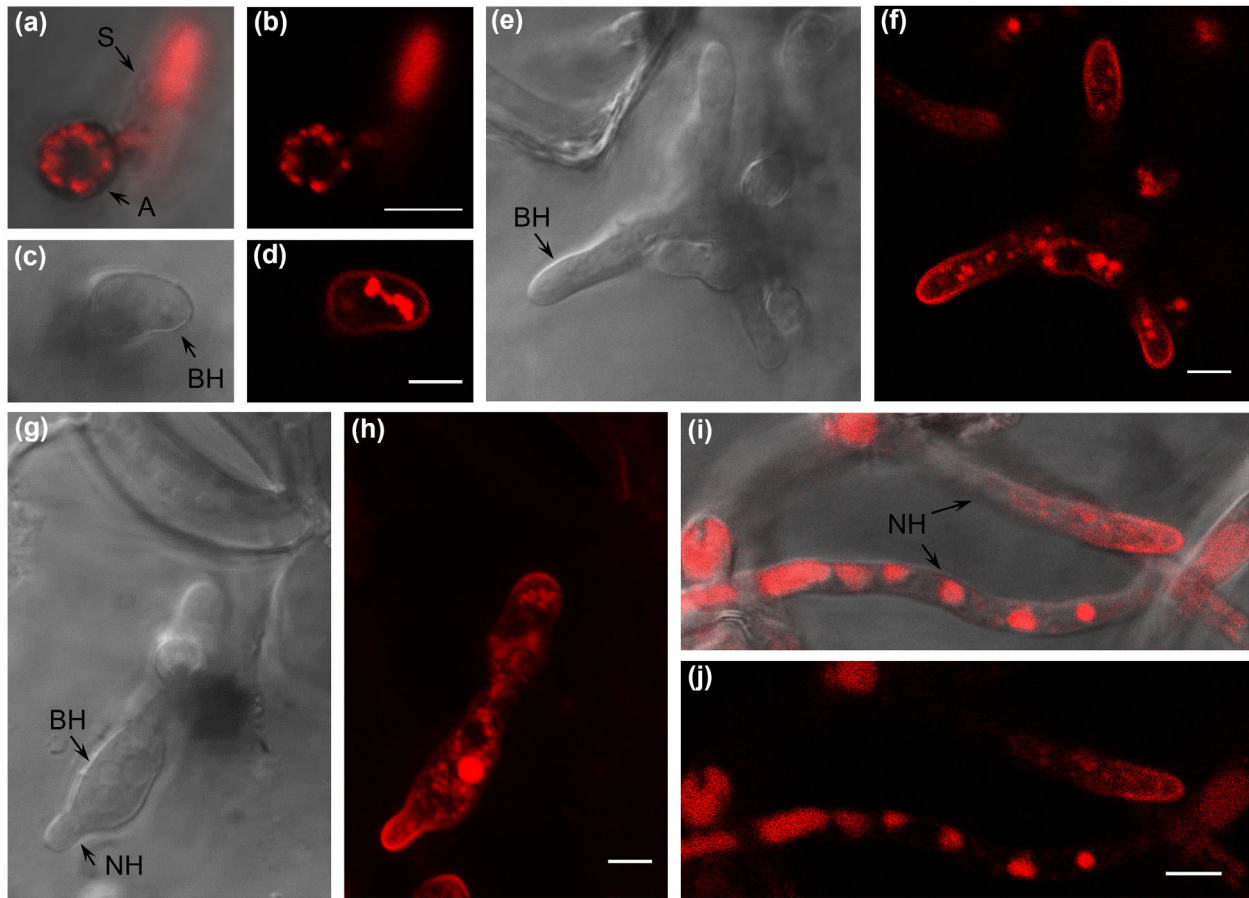


FIGURE 9 Localization of mScarlet-*ChSncl* in *C. higginsianum* infecting *Arabidopsis*. Fungal transformants expressing mScarlet-*ChSncl* were inoculated on *Arabidopsis* cotyledons and observed with confocal laser scanning microscopy. (a, b) mScarlet-*ChSncl* labelled vacuoles in spores and small punctae in appressoria. (c-f) In young biotrophic hyphae, mScarlet-*ChSncl* appeared to localize to the plasma membrane (PM) and small punctae. (g-h) At the transition to necrotrophy, mScarlet-*ChSncl* labelled the PMs of both biotrophic and necrotrophic hyphae. (I, J) In necrotrophic hyphae, mScarlet-*ChSncl* appeared to localize to the PM at hyphal tips and strongly labelled vacuoles. (b, d, f, h, j) fluorescence channel; (c, e, g) DIC channel; (a, i) Overlays of DIC and fluorescence channels. Scale bars = 5 μm . S, spore; A, appressorium; BH, biotrophic hypha; NH, necrotrophic hypha

2018). Approximately, 54% of apoplastic proteins secreted by the maize root pathogen *Trichoderma virens* lack a signal peptide (Nogueira-Lopez et al., 2018). The same is true for 48% of the total secretome of *M. oryzae* (Kim et al., 2013). As a form of unconventional secretion, EVs represent an attractive mechanism for the release of important fungal virulence factors. EVs are frequently observed by TEM at the interface between plant and fungal cells (Ivanov et al., 2019; Micali et al., 2011; Roth et al., 2019). Recent studies also suggest that EVs from fungal phytopathogens carry protein effectors and phytotoxic compounds (Bleackley et al., 2019; Garcia-Ceron et al., 2021; Garcia-Ceron et al., 2021).

To better understand the composition and function of EVs from plant fungal pathogens, we developed methods for isolating EVs from the hemibiotrophic pathogen, *C. higginsianum*. Our TEM analysis revealed EVs in the paramural space of biotrophic hyphae growing *in planta*, but attempts to isolate these structures from the supernatant of liquid cultured mycelia resulted in few if any particles. In order to isolate large numbers of vesicles from the supernatant, we found it necessary to first degrade the fungal cell wall with a mixture of β -glucanases. This suggests that *C. higginsianum* EVs do not pass efficiently through the fungal cell wall. Alternatively, these EVs may not cross the cell wall at all. They could instead function as a mechanism for bulk export to the paramural space, where they subsequently rupture, releasing their contents.

Extracellular vesicles were previously isolated from protoplasts of *Aspergillus fumigatus* by Rizzo et al. (2020). In that study, EVs were actively released from protoplasts, especially under conditions that favoured cell wall regeneration. Earlier studies have also observed the release of vesicles from protoplasts of *A. nidulans* and *Candida tropicalis* (Gibson & Peberdy, 1972; Osumi, 1998). It is unknown whether the EVs collected from *C. higginsianum* protoplasts were actively produced in response to the loss of the cell wall or if they were passively released from the space between the plasma membrane and cell wall after the latter's removal. We believe these vesicles are true EVs and are not artifacts produced from burst hyphal tips or damaged protoplasts for the following reasons: the supernatant obtained from cultures of intact mycelia did not contain significant levels of particles

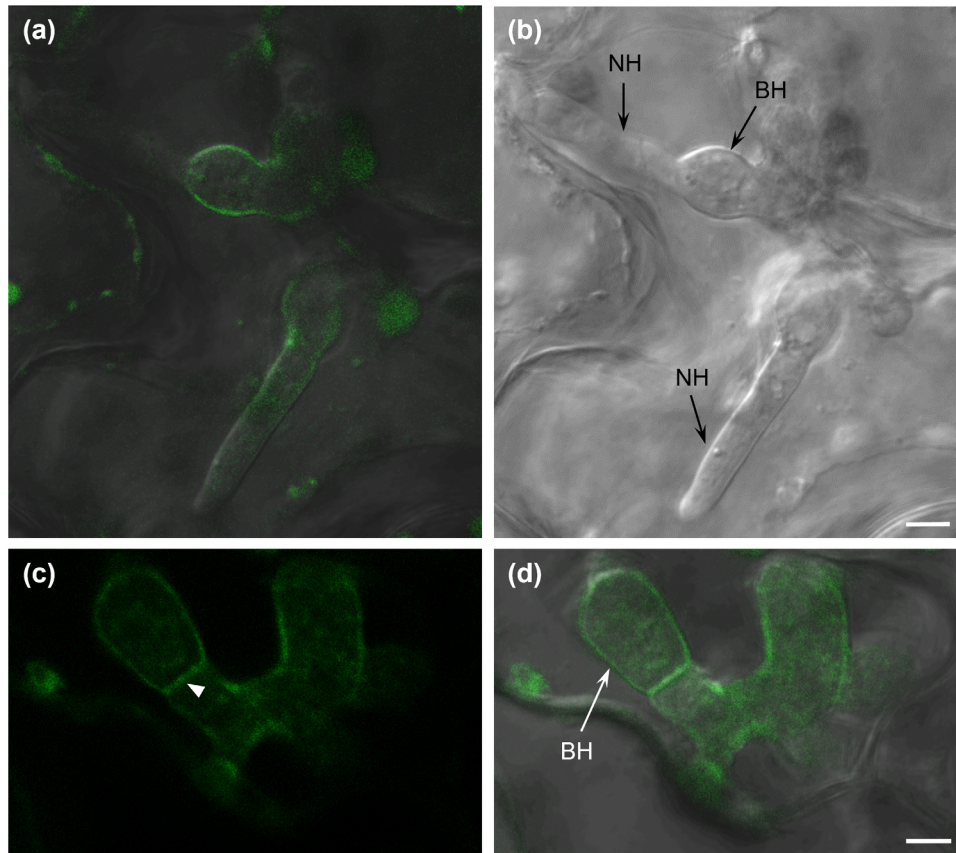


FIGURE 10 Localization of mNeonGreen-*ChSso2* in *C. higginsianum* infecting Arabidopsis. Fungal transformants expressing mNeonGreen-*ChSso2* were inoculated on Arabidopsis cotyledons and observed with confocal laser scanning microscopy. In biotrophic hyphae (BH), mNeonGreen-*ChSso2* appeared to localize to the plasma membrane (PM) as well as to septa (arrowhead). PM labelling appeared weaker in necrotrophic hyphae (NH) than in biotrophic hyphae. (a, d) Overlays of DIC and fluorescence channels; (b) DIC channel; (c) fluorescence channel. Scale bars = 5 μ m

(Figure 3), we observed very few dead protoplasts (Figure 4) and the contamination marker SOD2 was not detected in crude EV pellets (Figure 7).

Density gradient purification of *C. higginsianum* EV samples yielded two separate populations of vesicles, a low-density (LD) population at ~ 1.078 g/ml and a high density (HD) population at ~ 1.115 – 1.173 g/ml. These vesicles were approximately 100 nm in diameter and, using TEM, had a similar appearance to EVs isolated from other fungal phytopathogens (Bleackley et al., 2019; Hill & Solomon, 2020; Kwon et al., 2021). In examining the protein content of these vesicles, we treated the vesicles with trypsin and then purified them on a density gradient, removing extravesicular proteins through both enzymatic digestion and density purification.

Our proteomic analysis of *C. higginsianum* EVs identified a diverse set of proteins for both vesicle populations, including membrane transporters, small GTPases, chaperones and ribosomal subunits, as well as proteins involved in primary/secondary metabolism, cell redox homeostasis, vesicle-mediated transport and cytoskeletal organization. Over 50% of the proteins detected in each vesicle population were held in common. However, the LD population was more enriched for cytoplasmic elements while the HD vesicles were enriched for membrane-associated proteins and contained a higher percentage of proteins with predicted transmembrane domains. This difference could signify separate origins for each population. An enrichment in cytoplasmic elements might suggest that the vesicles formed inside the cell, similar to mammalian exosomes, while an enrichment in transmembrane proteins could indicate that vesicles were derived directly from the plasma membrane.

Among the membrane-associated proteins identified, we detected SNAREs and GTPases previously proposed as fungal EVs markers for *C. albicans* (Dawson et al., 2020). The proteomes also contained multiple proteins associated with cell wall biogenesis, suggesting that, similar to other species of fungi, *C. higginsianum* EVs may function in the formation or maintenance of this structure (Oliveira et al., 2010; Rizzo et al., 2020; Zhao et al., 2019). Interestingly, we also identified proteins encoded by previously identified secondary metabolite biosynthetic gene clusters (BGCs) involved in the synthesis of higginsianins (BGC16) and two other as-of-yet unidentified compounds (BGCs 21 and 71). Both BGC16 and BGC71 are transcriptionally induced during the biotrophic and necrotrophic phases of infection (Table S3 and Figure S4), suggesting that their metabolite products may contribute to fungal pathogenicity. Polyketide synthases have been found in the EVs of *Alternaria infectora* and *Fusarium oxysporum*

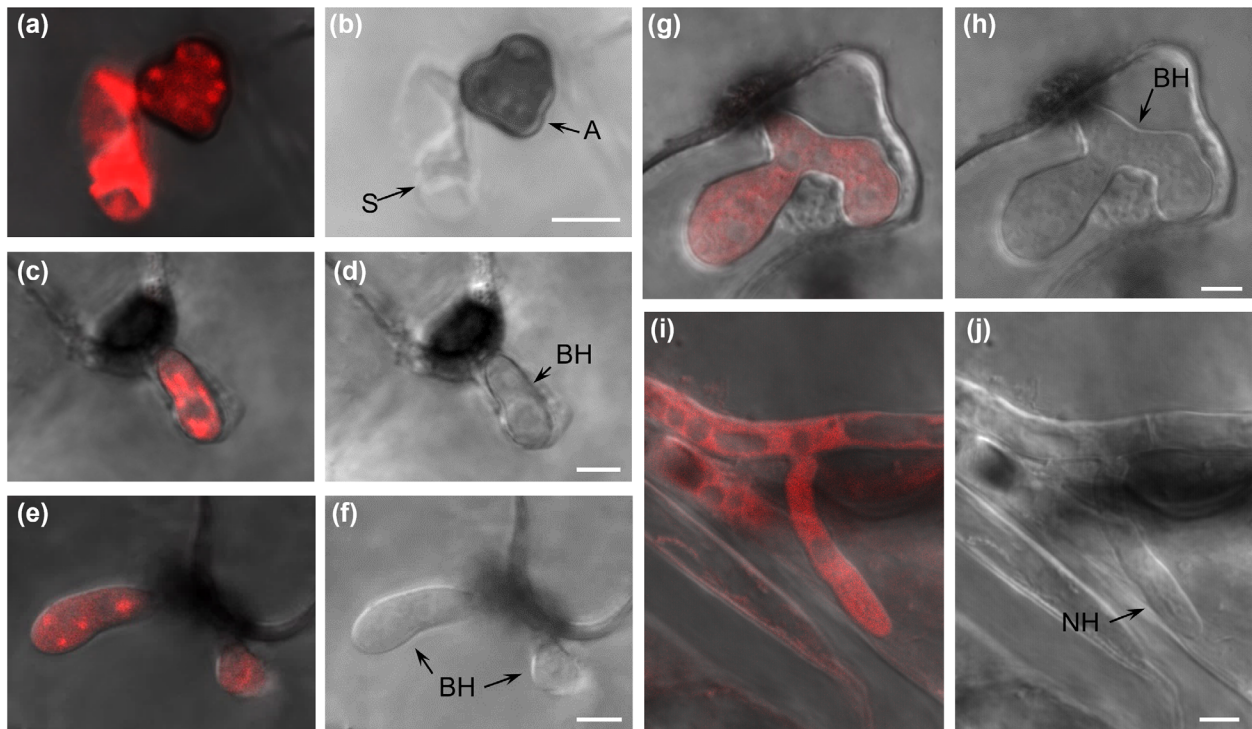


FIGURE 11 Localization of *ChBmh1*-mCherry in *C. higginsianum* infecting *Arabidopsis*. Fungal transformants expressing *ChBmh1*-mCherry were inoculated on *Arabidopsis* cotyledons and observed with confocal laser scanning microscopy. (a, b) *ChBmh1*-mCherry labelled vacuoles in spore and punctae in appressorium. (c-f) *ChBmh1*-mCherry localized to small punctae in young biotrophic hyphae. (g-j) In older biotrophic and necrotrophic hyphae, fluorescent labelling was distributed through the cytoplasm and excluded from vacuoles. (a, c, e, g, i) Overlays of DIC and fluorescence channels; b, d, f, h, j) DIC channel. Scale bars = 5 μ m. S, spore; A, appressorium; BH, biotrophic hypha; NH, necrotrophic hypha

f. sp. *vasinfectum*; EVs of the latter were also associated with an unidentified purple-coloured phytotoxic metabolite (Bleackley et al., 2019; Silva et al., 2014). Proteins involved in toxin synthesis were also identified in EVs from *Fusarium graminearum* (Garcia-Ceron et al., 2021). Combined, these findings suggest that EVs may represent a common mechanism among fungal phytopathogens for the export, or even extracellular synthesis, of biologically active metabolites. However, it should be noted that the transcriptome of axenically grown fungi differs considerably from fungal structures *in planta*. It is therefore likely the proteome of fungal EVs also changes during infection and that the secondary metabolite-related proteins detected in this study, with the possible exception of Higginsianin B, are expressed at higher levels *in vitro* than *in planta*.

From our list of EV proteins, we selected two SNARE proteins (*ChSnc1* and *ChSso2*) and one 14-3-3 protein (*ChBmh1*) to function as markers for the EV membrane and lumen, respectively. Orthologs of these proteins have been identified in EVs from multiple species of fungi (Bleackley et al., 2019; Dawson et al., 2020; Hill & Solomon, 2020; Rizzo et al., 2020; Wolf et al., 2014; Zhao et al., 2019). All three markers were detected in EV samples by immunoblot. *ChSnc1* and *ChSso2* were more enriched in EVs compared to total cell lysate, while the opposite was true for *ChBmh1*. Other studies have shown that EVs are often enriched for membrane proteins compared to soluble proteins, as the majority of their volume and surface area consists of lipid membrane (Bleackley et al., 2019). Moreover, a protease protection assay confirmed that all three markers were protected from digestion inside membranous compartments. In transgenic fungi grown on *Arabidopsis* leaves, we observed that *ChSnc1* was consistently localized to the apices of hyphae, known regions of secretion, while *ChBmh1* was more evenly distributed throughout the cytosol. Both markers localized to puncta inside appressoria. While fluorescent-tagged EV marker strains are available in yeasts (Dawson et al., 2020), to our knowledge, these are the first fluorescent EV marker strains for a filamentous plant pathogen. Though we could not detect extracellular signals with our current techniques, we hope these strains will prove valuable in the future for verifying EVs and tracking their release during infection. It is possible that these EVs are capable of moving beyond the fungal cell wall during infection, particularly in hyphal regions where the cell wall is thin (Kleemann et al., 2012; O'Connell et al., 2004). However, it could also be true that these vesicles function in the bulk export of proteins and other materials outside of the cell but never actually traverse the cell wall.

Fungal EVs are a rapidly growing field of study. While the majority of research has focused on human pathogens, there is a dawning appreciation for the role of EVs among fungal phytopathogens. We present here, for the first time, an analysis of EVs produced by the hemibiotrophic plant pathogen, *C. higginsianum*. We found it was necessary to generate protoplasts to isolate EVs. This suggests that *C. higginsianum* EVs do not efficiently pass through the cell wall of axenic mycelia. This is most likely a

problem common to all fungal EV studies. The majority of published fungal EV proteomes contain fewer than 100 proteins and sometimes pool EV samples from multiple independent replicates to achieve higher numbers (Bleackley et al., 2019; Bleackley et al., 2019). While the number of proteins detected depends on several factors ranging from the growth conditions to the type of equipment and software used for LC-MS/MS, the fungal cell wall undoubtedly represents an additional factor. It is already clear that external capsular structures are a barrier for the release of EVs from *C. neoformans* (Rodrigues et al., 2007). As previously suggested, protoplasting may therefore represent a more efficient way to determine the proteomes of fungal EVs (Rizzo et al., 2020).

Our research suggests that *C. higginsianum* releases EVs that could function in cell wall biogenesis and the export of secondary metabolites. The proteins *ChSnc1* and *ChBmh1* function as general markers for these vesicles and could be used in the future to verify and potentially track EVs produced by this fungus. These proteins are also attractive targets for genetic analysis, in order to determine how they impact the formation and contents of fungal EVs. Most excitingly, *C. higginsianum* is a pathogen of the model plant *Arabidopsis thaliana*, the EVs of which are currently the best-defined among plant species (Baldrich et al., 2019; Karimi et al., 2022; Rutter & Innes, 2017). Future research will need to determine if *C. higginsianum* releases larger numbers of EVs past the fungal cell wall during infection. The tools developed here could be used to verify the presence of fungal EVs or EV-delivered cargo in the plant extracellular spaces. This could in turn lead to an exploration of how fungal and plant EV contents change during different phases of infection. A solid understanding of EVs released by both pathogen and host paves the way for future studies examining EV interkingdom communication.

ACKNOWLEDGEMENTS

We thank the Indiana University Bloomington Light Microscopy Imaging Center and Electron Microscopy Center, as well as the INRAE Versailles Plant Cell Imaging Platform for access to light and electron microscopes. We also thank Dr. Jonathan Trinidad and the Laboratory for Mass Spectrometry at Indiana University for the proteomic analysis and help describing the methods involved. We are also grateful to Adeline Simon and the BIOGER bioinformatics platform for advice on gene ontology analysis. Richard O'Connell is supported by funding from the Agence Nationale de la Recherche (grant ANR-17-CAPS-0004-01). The INRAE BIOGER unit benefits from the support of the Saclay Plant Sciences-SPS (ANR-17-EUR-0007). Roger Innes is supported by funding from the United States National Science Foundation (grant numbers IOS-1645745 and IOS-1842685) and Department of Energy Office of Science (grant number 0000248555).

AUTHOR CONTRIBUTIONS

Brian D. Rutter: Conceptualization; Formal analysis; Investigation; Methodology; Visualization; Writing – original draft; Writing – review & editing. Thi-Thu-Huyen Chu: Formal analysis; Investigation; Methodology; Visualization; Writing – original draft; Writing – review & editing. Jean-Félix Dallery: Formal analysis; Visualization; Writing – original draft; Writing – review & editing. Kamil K. Zajt: Methodology. Richard J. O'Connell: Conceptualization; Funding acquisition; Project administration; Resources; Supervision; Writing – original draft; Writing – review & editing. Roger W. Innes: Conceptualization; Funding acquisition; Project administration; Resources; Supervision; Writing – original draft; Writing – review & editing.

CONFLICT OF INTEREST

The authors do not declare any conflicts of interest.


ORCID

Brian D. Rutter  <https://orcid.org/0000-0002-4354-9832>

Thi-Thu-Huyen Chu  <https://orcid.org/0000-0002-7011-0825>

Jean-Félix Dallery  <https://orcid.org/0000-0002-0771-9611>

Kamil K. Zajt  <https://orcid.org/0000-0003-3436-6097>

Richard J. O'Connell  <https://orcid.org/0000-0002-5358-6143>

Roger W. Innes  <https://orcid.org/0000-0001-9634-1413>

REFERENCES

- Aalto, M. K., Ronne, H., & Keranen, S. (1993). Yeast syntaxins Sso1p and Sso2p belong to a family of related membrane proteins that function in vesicular transport. *Embo Journal*, 12(11), 4095–4104. <https://www.ncbi.nlm.nih.gov/pubmed/8223426>
- Albuquerque, P. C., Nakayasu, E. S., Rodrigues, M. L., Frases, S., Casadevall, A., Zancope-Oliveira, R. M., Almeida, I. C., & Nosanchuk, J. D. (2008). Vesicular transport in *Histoplasma capsulatum*: An effective mechanism for trans-cell wall transfer of proteins and lipids in ascomycetes. *Cellular Microbiology*, 10(8), 1695–1710. <https://doi.org/10.1111/j.1462-5822.2008.01160.x>
- Almagro Armenteros, J. J., Tsirigos, K. D., Sonderby, C. K., Petersen, T. N., Winther, O., Brunak, S., von Heijne, G., & Nielsen, H. (2019). SignalP 5.0 improves signal peptide predictions using deep neural networks. *Nature Biotechnology*, 37(4), 420–423. <https://doi.org/10.1038/s41587-019-0036-z>
- Anderson, J., Mihalik, R., & Soll, D. R. (1990). Ultrastructure and antigenicity of the unique cell wall pimple of the *Candida* opaque phenotype. *Journal of Bacteriology*, 172(1), 224–235. <https://doi.org/10.1128/jb.172.1.224-235.1990>
- Baldrich, P., Rutter, B. D., Karimi, H. Z., Podicheti, R., Meyers, B. C., & Innes, R. W. (2019). Plant extracellular vesicles contain diverse small RNA species and are enriched in 10- to 17-nucleotide “Tiny” RNAs. *Plant Cell*, 31(2), 315–324. <https://doi.org/10.1105/tpc.18.00872>

- Bartnicki-Garcia, S., & Lippman, E. (1972). The bursting tendency of hyphal tips of fungi: Presumptive evidence for a delicate balance between wall synthesis and wall lysis in apical growth. *Microbiology (Reading, England)*, 73(3), 487–500. <https://doi.org/10.1099/00221287-73-3-487>
- Bernardo, S. M., Rane, H. S., Chavez-Dozal, A., & Lee, S. A. (2014). Secretion and filamentation are mediated by the *Candida albicans* t-SNAREs Sso2p and Sec9p. *Fems Yeast Research*, 14(5), 762–775. <https://doi.org/10.1111/1567-1364.12165>
- Bleackley, M. R., Dawson, C. S., & Anderson, M. A. (2019). Fungal extracellular vesicles with a focus on proteomic analysis. *Proteomics*, 19(8), e1800232. <https://doi.org/10.1002/pmic.201800232>
- Bleackley, M. R., Samuel, M., Garcia-Ceron, D., McKenna, J. A., Lowe, R. G. T., Pathan, M., Zhao, K., Ang, C. S., Mathivanan, S., & Anderson, M. A. (2019). Extracellular vesicles from the cotton pathogen *Fusarium oxysporum* f. sp. *vasinfectum* induce a phytotoxic response in plants. *Frontiers in Plant Science*, 10, 1610. <https://doi.org/10.3389/fpls.2019.01610>
- Bock, J. B., Matern, H. T., Peden, A. A., & Scheller, R. H. (2001). A genomic perspective on membrane compartment organization. *Nature*, 409(6822), 839–841. <https://doi.org/10.1038/35057024>
- Brennwald, P., Kearns, B., Champion, K., Keranen, S., Bankaitis, V., & Novick, P. (1994). Sec9 is a SNAP-25-like component of a yeast SNARE complex that may be the effector of Sec4 function in exocytosis. *Cell*, 79(2), 245–258. [https://doi.org/10.1016/0092-8674\(94\)90194-5](https://doi.org/10.1016/0092-8674(94)90194-5)
- Choi, D. S., Kim, D. K., Kim, Y. K., & Ghoo, Y. S. (2015). Proteomics of extracellular vesicles: Exosomes and ectosomes. *Mass Spectrometry Reviews*, 34(4), 474–490. <https://doi.org/10.1002/mas.21420>
- Cimmino, A., Mathieu, V., Masi, M., Baroncelli, R., Boari, A., Pescitelli, G., Ferderin, M., Lisy, R., Evidente, M., Tuzi, A., Zonno, M. C., Kornienko, A., Kiss, R., & Evidente, A. (2016). Higgsinsianins A and B, Two Diterpenoid alpha-Pyrone Produced by *Colletotrichum higgsinsianum*, with in Vitro Cytostatic Activity. *Journal of Natural Products*, 79(1), 116–125. <https://doi.org/10.1021/acs.jnatprod.5b00779>
- Collemare, J., O'Connell, R., & Lebrun, M. H. (2019). Nonproteinaceous effectors: The terra incognita of plant-fungal interactions. *The New phytologist*, 223(2), 590–596. <https://doi.org/10.1111/nph.15785>
- Dallery, J. F., Lapalu, N., Zampounis, A., Pigne, S., Luyten, I., Amselem, J., Wittenberg, A. H. J., Zhou, S., de Queiroz, M. V., Robin, G. P., Auger, A., Hainaut, M., Henrissat, B., Kim, K. T., Lee, Y. H., Lespinet, O., Schwartz, D. C., Thon, M. R., & O'Connell, R. J. (2017). Gapless genome assembly of *Colletotrichum higgsinsianum* reveals chromosome structure and association of transposable elements with secondary metabolite gene clusters. *Bmc Genomics [Electronic Resource]*, 18(1), 667. <https://doi.org/10.1186/s12864-017-4083-x>
- Dallery, J. F., Zimmer, M., Halder, V., Suliman, M., Pigne, S., Le Goff, G., Gianniu, D. D., Trougkos, I. P., Ouazzani, J., Gasperini, D., & O'Connell, R. J. (2020). Inhibition of jasmonate-mediated plant defences by the fungal metabolite higgsinsianin B. *Journal of Experimental Botany*, 71(10), 2910–2921. <https://doi.org/10.1093/jxb/eraa061>
- Dawson, C. S., Garcia-Ceron, D., Rajapaksha, H., Faou, P., Bleackley, M. R., & Anderson, M. A. (2020). Protein markers for *Candida albicans* EVs include claudin-like Sur7 family proteins. *Journal of extracellular vesicles*, 9(1), 1750810. <https://doi.org/10.1080/20013078.2020.1750810>
- de Jonge, R., van Esse, H. P., Kombrink, A., Shinya, T., Desaki, Y., Bours, R., van der Krol, S., Shibuya, N., Joosten, M. H., & Thomma, B. P. (2010). Conserved fungal LysM effector Ecp6 prevents chitin-triggered immunity in plants. *Science*, 329(5994), 953–955. <https://doi.org/10.1126/science.1190859>
- de Paula, R. G., Antonieto, A. C. C., Nogueira, K. M. V., Ribeiro, L. F. C., Rocha, M. C., Malavazi, I., Almeida, F., & Silva, R. N. (2019). Extracellular vesicles carry cellulases in the industrial fungus *Trichoderma reesei*. *Biotechnology for Biofuels*, 12, 146. <https://doi.org/10.1186/s13068-019-1487-7>
- Gaff, D. F., & Okong'O-Ogola, O. (1971). The use of non-permeating pigments for testing the survival of cells. *Journal of Experimental Botany*, 22(3), 756–758. <https://doi.org/10.1093/jxb/22.3.756>
- Garcia-Ceron, D., Dawson, C. S., Faou, P., Bleackley, M. R., & Anderson, M. A. (2021). Size-exclusion chromatography allows the isolation of EVs from the filamentous fungal plant pathogen *Fusarium oxysporum* f. sp. *vasinfectum* (Fov). *Proteomics*, 21(13-14), e2000240. <https://doi.org/10.1002/pmic.202000240>
- Garcia-Ceron, D., Lowe, R. G., McKenna, J. A., Brain, L. M., Dawson, C. S., Clark, B., Berkowitz, O., Faou, P., Whelan, J., Bleackley, M. R., & Anderson, M. A. (2021). Extracellular vesicles from *Fusarium graminearum* contain protein effectors expressed during infection of corn. *Journal of Fungi*, 7(11), 977. <https://doi.org/10.3390/jof7110977>
- Gelperin, D., Weigle, J., Nelson, K., Roseboom, P., Irie, K., Matsumoto, K., & Lemmon, S. (1995). 14-3-3 proteins: Potential roles in vesicular transport and Ras signaling in *Saccharomyces cerevisiae*. *PNAS*, 92(25), 11539–11543. <https://doi.org/10.1073/pnas.92.25.11539>
- Gibson, R. K., & Peberdy, J. F. (1972). Fine structure of protoplasts of *Aspergillus nidulans*. *Journal of General Microbiology*, 72(3), 529–538. <https://doi.org/10.1099/00221287-72-3-529>
- Gilchrist, C. L. M., Booth, T. J., van Wersch, B., van Grieken, L., Medema, M. H., & Chooi, Y. - H. (2021). cblaster: A remote search tool for rapid identification and visualization of homologous gene clusters. *Bioinformatics Advances*, 1(1), vbab016. <https://doi.org/10.1093/bioadv/vbab016>
- Gilchrist, C. L. M., & Chooi, Y. - H. (2021). clinker & clustermap.js: Automatic generation of gene cluster comparison figures. *Bioinformatics Advances*, 37, 3. <https://doi.org/10.1093/bioinformatics/btab007>
- Giraldo, M. C., Dagdas, Y. F., Gupta, Y. K., Mentlak, T. A., Yi, M., Martinez-Rocha, A. L., Saitoh, H., Terauchi, R., Talbot, N. J., & Valent, B. (2013). Two distinct secretion systems facilitate tissue invasion by the rice blast fungus *Magnaporthe oryzae*. *Nature Communication*, 4, 1996. <https://doi.org/10.1038/ncomms2996>
- Gupta, G. D., & Brent Heath, I. (2002). Predicting the distribution, conservation, and functions of SNAREs and related proteins in fungi. *Fungal Genetics and Biology*, 36(1), 1–21. [https://doi.org/10.1016/S1087-1845\(02\)00017-8](https://doi.org/10.1016/S1087-1845(02)00017-8)
- Hacquard, S., Kracher, B., Hiruma, K., Münch, P. C., Garrido-Oter, R., Thon, M. R., Weinmann, A., Damm, U., Dallery, J. - F., Hainaut, M., Henrissat, B., Lespinet, O., Sacristán, S., van Themaat, E. V. L., Kemen, E., McHardy, A. C., Schulze-Lefert, P., & O'Connell, R. J. (2016). Survival trade-offs in plant roots during colonization by a closely related beneficial and pathogenic fungi. *Nature Communication*, 7(1), 1–13. <https://doi.org/10.1038/ncomms11362>
- Hai, T. P., Tuan, T. L., Anh, D. V., Mai, T. N., Huong, L. N. P., Thwaites, G. E., Johnson, E., Chau, N. V. V., Ashton, P., & Day, J. (2020). The expression of virulence by the *Cryptococcus neoformans* VN1a-5 lineage is plastic and associated with host immune background. *bioRxiv*, <https://doi.org/10.1101/2020.02.24.962134>
- Hayakawa, Y., Ishikawa, E., Shoji, J. Y., Nakano, H., & Kitamoto, K. (2011). Septum-directed secretion in the filamentous fungus *Aspergillus oryzae*. *Molecular Microbiology*, 81(1), 40–55. <https://doi.org/10.1111/j.1365-2958.2011.07700.x>
- Hemetsberger, C., Herrberger, C., Zechmann, B., Hillmer, M., & Doehlemann, G. (2012). The *Ustilago maydis* effector Pep1 suppresses plant immunity by inhibition of host peroxidase activity. *Plos Pathogens*, 8(5), e1002684. <https://doi.org/10.1371/journal.ppat.1002684>
- Hickey, P. C., Swift, S. R., Roca, M. G., & Read, N. D. (2004). Live-cell Imaging of Filamentous Fungi Using Vital Fluorescent Dyes and Confocal Microscopy. *In Methods in Microbiology*, 34, 63–87. [https://doi.org/10.1016/S0580-9517\(04\)34003-1](https://doi.org/10.1016/S0580-9517(04)34003-1)
- Hill, E. H., & Solomon, P. S. (2020). Extracellular vesicles from the apoplastic fungal wheat pathogen *Zymoseptoria tritici*. *Fungal Biology and Biotechnology*, 7(13), 1–14. <https://doi.org/10.1186/s40694-020-00103-2>
- Huang, S. H., Wu, C. H., Chang, Y. C., Kwon-Chung, K. J., Brown, R. J., & Jong, A. (2012). *Cryptococcus neoformans*-derived microvesicles enhance the pathogenesis of fungal brain infection. *Plos One*, 7(11), e48570. <https://doi.org/10.1371/journal.pone.0048570>

- Huser, A., Takahara, H., Schmalenbach, W., & O'Connell, R. (2009). Discovery of pathogenicity genes in the crucifer anthracnose fungus *Colletotrichum higginsianum*, using random insertional mutagenesis. *Molecular Plant-microbe Interactions : MPMI*, 22(2), 143–156. <https://doi.org/10.1094/MPMI-22-2-0143>
- Ikedda, M. A. K., de Almeida, J. R. F., Jannuzzi, G. P., Cronemberger-Andrade, A., Torrecilhas, A. C. T., Moretti, N. S., da Cunha, J. P. C., de Almeida, S. R., & Ferreira, K. S. (2018). Extracellular vesicles from *Sporothrix brasiliensis* are an important virulence factor that induce an increase in fungal burden in experimental sporotrichosis. *Frontiers in Microbiology*, 9, 2286. <https://doi.org/10.3389/fmicb.2018.02286>
- Ivanov, S., Austin, J. 2nd, Berg, R. H., & Harrison, M. J. (2019). Extensive membrane systems at the host-arbuscular mycorrhizal fungus interface. *Nature Plants*, 5(2), 194–203. <https://doi.org/10.1038/s41477-019-0364-5>
- Jashni, M. K., Dols, I. H., Iida, Y., Boeren, S., Beenen, H. G., Mehrabi, R., Collemare, J., & de Wit, P. J. (2015). Synergistic action of a metalloprotease and a serine protease from *Fusarium oxysporum* f. sp. *lycopersici* cleaves chitin-binding tomato chitinases, reduces their antifungal activity, and enhances fungal virulence. *Molecular Plant-microbe Interactions : MPMI*, 28(9), 996–1008. <https://doi.org/10.1094/MPMI-04-15-0074-R>
- Karimi, H. Z., Baldrich, P., Rutter, B. D., Borniego, L., Zajt, K. K., Meyers, B. C., & Innes, R. W. (2022). Arabidopsis apoplastic fluid contains sRNA- and circular RNA-protein complexes that are located outside extracellular vesicles. *Plant Cell*, <https://doi.org/10.1093/plcell/koac043>
- Kautsar, S. A., Blin, K., Shaw, S., Navarro-Munoz, J. C., Terlouw, B. R., van der Hoof, J. J. J., van Santen, J. A., Tracanna, V., Suarez Duran, H. G., Pascal Andreu, V., Selem-Mojica, N., Alanjary, M., Robinson, S. L., Lund, G., Epstein, S. C., Sisto, A. C., Charkoudian, L. K., Collemare, J., Linington, R. G., & ... Medema, M. H. (2020). MIBiG 2.0: A repository for biosynthetic gene clusters of known function. *Nucleic Acids Research*, 48(D1), D454–D458. <https://doi.org/10.1093/nar/gkz882>
- Kim, S. G., Wang, Y., Lee, K. H., Park, Z. Y., Park, J., Wu, J., Kwon, S. J., Lee, Y. H., Agrawal, G. K., Rakwal, R., Kim, S. T., & Kang, K. Y. (2013). In-depth insight into in vivo apoplastic secretome of rice-Magnaporthe oryzae interaction. *Journal of Proteomics*, 78, 58–71. <https://doi.org/10.1016/j.jprot.2012.10.029>
- Kleemann, J., Rincon-Rivera, L. J., Takahara, H., Neumann, U., van Themaat, E. V. L., van der Does, H. C., Hacquard, S., Stüber, K., Will, I., Schmalenbach, W., Schmelzer, E., & O'Connell, R. J. (2012). Sequential delivery of host-induced virulence effectors by appressoria and intracellular hyphae of the phytopathogen *Colletotrichum higginsianum*. *PLoS pathogens*, 8(4), e1002643. <https://doi.org/10.1371/journal.ppat.1002643>
- Klopper, T. H., Kienle, C. N., & Fasshauer, D. (2007). An elaborate classification of SNARE proteins sheds light on the conservation of the eukaryotic endomembrane system. *Molecular Biology of the Cell*, 18(9), 3463–3471. <https://doi.org/10.1091/mbc.e07-03-0193>
- Krijger, J. J., Thon, M. R., Deising, H. B., & Wirsal, S. G. (2014). Compositions of fungal secretomes indicate a greater impact of phylogenetic history than lifestyle adaptation. *Bmc Genomics [Electronic Resource]*, 15(722), 1–19. <https://doi.org/10.1186/1471-2164-15-722>
- Krogh, A., Larsson, B., von Heijne, G., & Sonnhammer, E. L. (2001). Predicting transmembrane protein topology with a hidden Markov model: Application to complete genomes. *Journal of Molecular Biology*, 305(3), 567–580. <https://doi.org/10.1006/jmbi.2000.4315>
- Kubicek, C. P., Starr, T. L., & Glass, N. L. (2014). Plant cell wall-degrading enzymes and their secretion in plant-pathogenic fungi. *Annual Review of Phytopathology*, 52, 427–451. <https://doi.org/10.1146/annurev-phyto-102313-045831>
- Kumar, R. (2017). An account of fungal 14-3-3 proteins. *European Journal of Cell Biology*, 96(2), 206–217. <https://doi.org/10.1016/j.ejcb.2017.02.006>
- Kuratsu, M., Taura, A., Shoji, J. Y., Kikuchi, S., Arioka, M., & Kitamoto, K. (2007). Systematic analysis of SNARE localization in the filamentous fungus *Aspergillus oryzae*. *Fungal Genetics and Biology*, 44(12), 1310–1323. <https://doi.org/10.1016/j.fgb.2007.04.012>
- Kwon, S., Rupp, O., Brachmann, A., Blum, C. F., Kraege, A., Goesmann, A., & Feldbrugge, M. (2021). mRNA Inventory of Extracellular Vesicles from *Ustilago maydis*. *Journal of Fungi (Basel)*, 7(7), 562. <https://doi.org/10.3390/jof7070562>
- Lambou, K., Tharreau, D., Kohler, A., Sirven, C., Marguerettaz, M., Barbisan, C., Sexton, A. C., Kellner, E. M., Martin, F., Howlett, B. J., Orbach, M. J., & Lebrun, M. H. (2008). Fungi have three tetraspanin families with distinct functions. *Bmc Genomics [Electronic Resource]*, 9(63), 1–14. <https://doi.org/10.1186/1471-2164-9-63>
- Latge, J. P. (2007). The cell wall: A carbohydrate armour for the fungal cell. *Molecular Microbiology*, 66(2), 279–290. <https://doi.org/10.1111/j.1365-2958.2007.05872.x>
- Littlejohn, G. R., Mansfield, J. C., Christmas, J. T., Witterick, E., Fricker, M. D., Grant, M. R., Smirnov, N., Everson, R. M., Moger, J., & Love, J. (2014). An update: Improvements in imaging perfluorocarbon-mounted plant leaves with implications for studies of plant pathology, physiology, development and cell biology. *Frontiers in Plant Science*, 5, 140. <https://doi.org/10.3389/fpls.2014.00140>
- Marina, C. L., Burgel, P. H., Agostinho, D. P., Zamith-Miranda, D., Las-Casas, L. O., Tavares, A. H., Nosanchuk, J. D., & Bocca, A. L. (2020). Nutritional conditions modulate *C. neoformans* extracellular vesicles' capacity to elicit host immune response. *Microorganisms*, 8(11), 1815. <https://doi.org/10.3390/microorganisms8111815>
- Matos Baltazar, L., Nakayasu, E. S., Sobreira, T. J., Choi, H., Casadevall, A., Nimrichter, L., & Nosanchuk, J. D. (2016). Antibody binding alters the characteristics and contents of extracellular vesicles released by *histoplasma capsulatum*. *mSphere*, 1(2), e00085-15. <https://doi.org/10.1128/mSphere.00085-15>
- McCotter, S. W., Horianopoulos, L. C., & Kronstad, J. W. (2016). Regulation of the fungal secretome. *Current Genetics*, 62(3), 533–545. <https://doi.org/10.1007/s00294-016-0578-2>
- Micali, C. O., Neumann, U., Grunewald, D., Panstruga, R., & O'Connell, R. (2011). Biogenesis of a specialized plant-fungal interface during host cell internalization of *Golovinomyces orontii* haustoria. *Cellular Microbiology*, 13(2), 210–226. <https://doi.org/10.1111/j.1462-5822.2010.01530.x>
- Motteram, J., Lovegrove, A., Pirie, E., Marsh, J., Devonshire, J., van de Meene, A., Hammond-Kosack, K., & Rudd, J. J. (2011). Aberrant protein N-glycosylation impacts upon infection-related growth transitions of the haploid plant-pathogenic fungus *Mycosphaerella graminicola*. *Molecular Microbiology*, 81(2), 415–433. <https://doi.org/10.1111/j.1365-2958.2011.07701.x>
- Naumann, T. A., & Price, N. P. J. (2012). Truncation of class IV chitinases from Arabidopsis by secreted fungal proteases. *Molecular Plant Pathology*, 13(9), 1135–1139. <https://doi.org/10.1111/j.1364-3703.2012.00805.x>
- Naumann, T. A., & Wicklow, D. T. (2010). Allozyme-specific modification of a maize seed chitinase by a protein secreted by the fungal pathogen *Stenocarpella maydis*. *Phytopathology*, 100(7), 645–654. <https://doi.org/10.1094/PHYTO-100-7-0645>
- Naumann, T. A., Wicklow, D. T., & Kendra, D. F. (2009). Maize seed chitinase is modified by a protein secreted by *Bipolaris zeicola*. *Physiological and Molecular Plant Pathology*, 74(2), 134–141. <https://doi.org/10.1016/j.pmp.2009.10.004>
- Naumann, T. A., Wicklow, D. T., & Price, N. P. J. (2011). Identification of a chitinase-modifying protein from *Fusarium verticillioides*: Truncation of a host resistance protein by a fungalysin metalloprotease. *Journal of Biological Chemistry*, 286(41), 35358–35366. <https://doi.org/10.1074/jbc.M111.279646>
- Nogueira-Lopez, G., Greenwood, D. R., Middleditch, M., Winefield, C., Eaton, C., Steyaert, J. M., & Mendoza-Mendoza, A. (2018). The Apoplastic Secretome of *trichoderma virens* during interaction with maize roots shows an inhibition of plant defence and scavenging oxidative stress secreted proteins. *Frontiers in Plant Science*, 9, 409. <https://doi.org/10.3389/fpls.2018.00409>
- O'Connell, R., Herbert, C., Sreenivasaprasad, S., Khatib, M., Esquerre-Tugay, M. T., & Dumas, B. (2004). A novel Arabidopsis-*Colletotrichum* pathosystem for the molecular dissection of plant-fungal interactions. *Molecular Plant-microbe Interactions : MPMI*, 17(3), 272–282. <https://doi.org/10.1094/MPMI.2004.17.3.272>

- O'Connell, R. J., Thon, M. R., Hacquard, S., Amyotte, S. G., Kleemann, J., Torres, M. F., Damm, U., Buiate, E. A., Epstein, L., Alkan, N., Altmüller, J., Alvarado-Balderrama, L., Bauser, C. A., Becker, C., Birren, B. W., Chen, Z., Choi, J., Crouch, J. A., Duvick, J. P., & Vaillancourt, L. J. (2012). Lifestyle transitions in plant pathogenic *Colletotrichum* fungi deciphered by genome and transcriptome analyses. *Nature Genetics*, *44*(9), 1060–1065. <https://doi.org/10.1038/ng.2372>
- O'Mara, S. P., Broz, K., Boenisch, M., Zhong, Z., Dong, Y., & Kistler, H. C. (2020). The Fusarium graminearum t-SNARE Sso2 is involved in growth, defense, and DON accumulation and virulence. *Molecular Plant-microbe Interactions : MPMI*, *33*(7), 888–901. <https://doi.org/10.1094/MPMI-01-20-0012-R>
- Oliveira, D. L., Freire-de-Lima, C. G., Nosanchuk, J. D., Casadevall, A., Rodrigues, M. L., & Nimrichter, L. (2010). Extracellular vesicles from *Cryptococcus neoformans* modulate macrophage functions. *Infection and Immunity*, *78*(4), 1601–1609. <https://doi.org/10.1128/IAI.01171-09>
- Osumi, M. (1998). The ultrastructure of yeast: Cell wall structure and formation. *Micron (Oxford, England: 1993)*, *29*(2-3), 207–233. [https://doi.org/10.1016/s0968-4328\(97\)00072-3](https://doi.org/10.1016/s0968-4328(97)00072-3)
- Peberdy, J. F. (1994). Protein secretion in filamentous fungi—trying to understand a highly productive black box. *Trends in Biotechnology*, *12*(2), 50–57. [https://doi.org/10.1016/0167-7799\(94\)90100-7](https://doi.org/10.1016/0167-7799(94)90100-7)
- Peng, X. L., Xu, W. T., Wang, Y., Huang, K. L., Liang, Z. H., Zhao, W. W., & Luo, Y. B. (2010). Mycotoxin Ochratoxin A-induced cell death and changes in oxidative metabolism of *Arabidopsis thaliana*. *Plant Cell Reports*, *29*(2), 153–161. <https://doi.org/10.1007/s00299-009-0808-x>
- Peres da Silva, R., Puccia, R., Rodrigues, M. L., Oliveira, D. L., Joffe, L. S., Cesar, G. V., Nimrichter, L., Goldenberg, S., & Alves, L. R. (2015). Extracellular vesicle-mediated export of fungal RNA. *Science Reports*, *5*, 7763. <https://doi.org/10.1038/srep07763>
- Pradhan, A., Ghosh, S., Sahoo, D., & Jha, G. (2021). Fungal effectors, the double edge sword of phytopathogens. *Current Genetics*, *67*(1), 27–40. <https://doi.org/10.1007/s00294-020-01118-3>
- Priebe, S., Kreisel, C., Horn, F., Guthke, R., & Linde, J. (2015). FungiFun2: A comprehensive online resource for systematic analysis of gene lists from fungal species. *Bioinformatics*, *31*(3), 445–446. <https://doi.org/10.1093/bioinformatics/btu627>
- Pusztahelyi, T., Imre, H. J., & Pócsi, I. (2015). Secondary metabolites in fungus-plant interactions. *Frontiers in Plant Science*, *6*, 573. <https://doi.org/10.3389/fpls.2015.00573>
- Rabouille, C. (2017). Pathways of unconventional protein secretion. *Trends in Cell Biology*, *27*(3), 230–240. <https://doi.org/10.1016/j.tcb.2016.11.007>
- Rizuelme, M., & Sanchez-Leon, E. (2014). The Spitzenkörper: A choreographer of fungal growth and morphogenesis. *Current Opinion in Microbiology*, *20*, 27–33. <https://doi.org/10.1016/j.mib.2014.04.003>
- Rizzo, J., Chaze, T., Miranda, K., Roberson, R. W., Gorgette, O., Nimrichter, L., Matondo, M., Latge, J. P., Beauvais, A., & Rodrigues, M. L. (2020). Characterization of extracellular vesicles produced by *aspergillus fumigatus* protoplasts. *mSphere*, *5*(4), e00476–20. <https://doi.org/10.1128/mSphere.00476-20>
- Rizzo, J., Wong, S. S. W., Gazi, A. D., Moyrand, F., Chaze, T., Commere, P. H., Novault, S., Matondo, M., Pehau-Arnaudet, G., Reis, F. C. G., Vos, M., Alves, L. R., May, R. C., Nimrichter, L., Rodrigues, M. L., Aimaniananda, V., & Janbon, G. (2021). *Cryptococcus* extracellular vesicles properties and their use as vaccine platforms. *Journal of extracellular vesicles*, *10*(10), e12129. <https://doi.org/10.1002/jev.21219>
- Rodrigues, M. L., Franzen, A. J., Nimrichter, L., & Miranda, K. (2013). Vesicular mechanisms of traffic of fungal molecules to the extracellular space. *Current Opinion in Microbiology*, *16*(4), 414–420. <https://doi.org/10.1016/j.mib.2013.04.002>
- Rodrigues, M. L., Nimrichter, L., Oliveira, D. L., Frases, S., Miranda, K., Zaragoza, O., Alvarez, M., Nakouzi, A., Feldmesser, M., & Casadevall, A. (2007). Vesicular polysaccharide export in *Cryptococcus neoformans* is a eukaryotic solution to the problem of fungal trans-cell wall transport. *Eukaryotic Cell*, *6*(1), 48–59. <https://doi.org/10.1128/EC.00318-06>
- Rossi, G., Salminen, A., Rice, L. M., Brunger, A. T., & Brennwald, P. (1997). Analysis of a yeast SNARE complex reveals remarkable similarity to the neuronal SNARE complex and a novel function for the C terminus of the SNAP-25 homolog, Sec9. *Journal of Biological Chemistry*, *272*(26), 16610–16617. <https://doi.org/10.1074/jbc.272.26.16610>
- Roth, D., Birkenfeld, J., & Betz, H. (1999). Dominant-negative alleles of 14-3-3 proteins cause defects in actin organization and vesicle targeting in the yeast *Saccharomyces cerevisiae*. *Febs Letters*, *460*(3), 411–416. [https://doi.org/10.1016/s0014-5793\(99\)01383-6](https://doi.org/10.1016/s0014-5793(99)01383-6)
- Roth, R., Hillmer, S., Funaya, C., Chiappello, M., Schumacher, K., Lo Presti, L., Kahmann, R., & Paszkowski, U. (2019). Arbuscular cell invasion coincides with extracellular vesicles and membrane tubules. *Nature Plants*, *5*(2), 204–211. <https://doi.org/10.1038/s41477-019-0365-4>
- Rutter, B. D., & Innes, R. W. (2017). Extracellular vesicles isolated from the leaf apoplast carry stress-response proteins. *Plant Physiology*, *173*(1), 728–741. <https://doi.org/10.1104/pp.16.01253>
- Sangermano, F., Masi, M., Vivo, M., Ravindra, P., Cimmino, A., Pollice, A., Evidente, A., & Calabro, V. (2019). Higgsianins A and B, two fungal diterpenoid alpha-pyrones with cytotoxic activity against human cancer cells. *Toxicology in Vitro*, *61*, 104614. <https://doi.org/10.1016/j.tiv.2019.104614>
- Shoji, J. Y., Kikuma, T., & Kitamoto, K. (2014). Vesicle trafficking, organelle functions, and unconventional secretion in fungal physiology and pathogenicity. *Current Opinion in Microbiology*, *20*, 1–9. <https://doi.org/10.1016/j.mib.2014.03.002>
- Silva, B. M., Prados-Rosales, R., Espadas-Moreno, J., Wolf, J. M., Luque-Garcia, J. L., Goncalves, T., & Casadevall, A. (2014). Characterization of *Alternaria infectoria* extracellular vesicles. *Medical Mycology*, *52*(2), 202–210. <https://doi.org/10.1093/mmy/myt003>
- Sonnhammer, E. L., von Heijne, G., & Krogh, A. (1998). A hidden Markov model for predicting transmembrane helices in protein sequences. *Proceedings International Conference on Intelligent Systems for Molecular Biology*, *6*, 175–182. <https://www.ncbi.nlm.nih.gov/pubmed/9783223>
- Takahara, H., Dolf, A., Endl, E., & O'Connell, R. (2009). Flow cytometric purification of *Colletotrichum higginsianum* biotrophic hyphae from *Arabidopsis* leaves for stage-specific transcriptome analysis. *Plant Journal*, *59*(4), 672–683. <https://doi.org/10.1111/j.1365-313X.2009.03896.x>
- Takeo, K., Uesaka, I., Uehira, K., & Nishiura, M. (1973). Fine structure of *Cryptococcus neoformans* grown in vivo as observed by freeze-etching. *Journal of Bacteriology*, *113*(3), 1449–1454. <https://doi.org/10.1128/jb.113.3.1449-1454.1973>
- Tanaka, S., Yamada, K., Yabumoto, K., Fujii, S., Huser, A., Tsuji, G., Koga, H., Dohi, K., Mori, M., Shiraishi, T., O'Connell, R., & Kubo, Y. (2007). *Saccharomyces cerevisiae* SSD1 orthologues are essential for host infection by the ascomycete plant pathogens *Colletotrichum lagenarium* and *Magnaporthe grisea*. *Molecular Microbiology*, *64*(5), 1332–1349. <https://doi.org/10.1111/j.1365-2958.2007.05742.x>
- Valkonen, M., Kalkman, E. R., Saloheimo, M., Penttilä, M., Read, N. D., & Duncan, R. R. (2007). Spatially segregated SNARE protein interactions in living fungal cells. *Journal of Biological Chemistry*, *282*(31), 22775–22785. <https://doi.org/10.1074/jbc.M700916200>
- Vallejo, M. C., Nakayasu, E. S., Longo, L. V., Ganiko, L., Lopes, F. G., Matsuo, A. L., Almeida, I. C., & Puccia, R. (2012). Lipidomic analysis of extracellular vesicles from the pathogenic phase of *Paracoccidioides brasiliensis*. *Plos One*, *7*(6), e39463. <https://doi.org/10.1371/journal.pone.0039463>
- van Esse, H. P., Bolton, M. D., Stergiopoulos, I., de Wit, P. J., & Thomma, B. P. (2007). The chitin-binding *Cladosporium fulvum* effector protein Avr4 is a virulence factor. *Molecular plant-microbe interactions : MPMI*, *20*(9), 1092–1101. <https://doi.org/10.1094/MPMI-20-9-1092>
- van Esse, H. P., Van't Klooster, J. W., Bolton, M. D., Yadeta, K. A., van Baarlen, P., Boeren, S., Vervoort, J., de Wit, P. J., & Thomma, B. P. (2008). The *Cladosporium fulvum* virulence protein Avr2 inhibits host proteases required for basal defense. *Plant Cell*, *20*(7), 1948–1963. <https://doi.org/10.1105/tpc.108.059394>
- van Heusden, G. P., & Steensma, H. Y. (2006). Yeast 14-3-3 proteins. *Yeast*, *23*(3), 159–171. <https://doi.org/10.1002/yea.1338>

- van Niel, G., D'Angelo, G., & Raposo, G. (2018). Shedding light on the cell biology of extracellular vesicles. *Nature Reviews Molecular Cell Biology*, 19(4), 213–228. <https://doi.org/10.1038/nrm.2017.125>
- Vargas, G., Rocha, J. D., Oliveira, D. L., Albuquerque, P. C., Frases, S., Santos, S. S., Nosanchuk, J. D., Gomes, A. M., Medeiros, L. C., Miranda, K., Sobreira, T. J., Nakayasu, E. S., Arigi, E. A., Casadevall, A., Guimaraes, A. J., Rodrigues, M. L., Freire-de-Lima, C. G., Almeida, I. C., & Nimrichter, L. (2015). Compositional and immunobiological analyses of extracellular vesicles released by *Candida albicans*. *Cellular Microbiology*, 17(3), 389–407. <https://doi.org/10.1111/cmi.12374>
- Wang, J., Tian, L., Zhang, D. D., Short, D. P. G., Zhou, L., Song, S. S., Liu, Y., Wang, D., Kong, Z. Q., Cui, W. Y., Ma, X. F., Klosterman, S. J., Subbarao, K. V., Chen, J. Y., & Dai, X. F. (2018). SNARE-encoding genes *VdSec22* and *VdSso1* mediate protein secretion required for full virulence in *Verticillium dahliae*. *Molecular plant-microbe interactions : MPMI*, 31(6), 651–664. <https://doi.org/10.1094/MPMI-12-17-0289-R>
- Woith, E., Fuhrmann, G., & Melzig, M. F. (2019). Extracellular vesicles-connecting kingdoms. *International Journal of Molecular Sciences*, 20(22), 5695. <https://doi.org/10.3390/ijms20225695>
- Wolf, J. M., Espadas-Moreno, J., Luque-Garcia, J. L., & Casadevall, A. (2014). Interaction of *Cryptococcus neoformans* extracellular vesicles with the cell wall. *Eukaryotic cell*, 13(12), 1484–1493. <https://doi.org/10.1128/EC.00111-14>
- Yanez-Mo, M., Siljander, P. R., Andreu, Z., Zavec, A. B., Borrás, F. E., Buzas, E. I., Buzas, K., Casal, E., Cappello, F., Carvalho, J., Colas, E., Silva, C. -, A, F, S, F. -, P, J, M., Ghobrial, I. M., Giebel, B., Gimona, M., Graner, M., ... De Wever, O. (2015). Biological properties of extracellular vesicles and their physiological functions. *Journal of extracellular vesicles*, 4, 27066. <https://doi.org/10.3402/jev.v4.27066>
- Zarnowski, R., Sanchez, H., Covelli, A. S., Dominguez, E., Jaromin, A., Bernhardt, J., Mitchell, K. F., Heiss, C., Azadi, P., Mitchell, A., & Andes, D. R. (2018). *Candida albicans* biofilm-induced vesicles confer drug resistance through matrix biogenesis. *Plos Biology*, 16(10), e2006872. <https://doi.org/10.1371/journal.pbio.2006872>
- Zhao, K., Bleackley, M., Chisanga, D., Gangoda, L., Fonseka, P., Liem, M., Kalra, H., Saffar, Al, H, K, S, A., C, S., Adda, C. G., Jiang, L., Yap, K., Poon, I. K., Lock, P., Bulone, V., Anderson, M., & Mathivanan, S. (2019). Extracellular vesicles secreted by *Saccharomyces cerevisiae* are involved in cell wall remodelling. *Communications Biology*, 2, 305. <https://doi.org/10.1038/s42003-019-0538-8>
- Zheng, W., Lin, Y., Fang, W., Zhao, X., Lou, Y., Wang, G., Zheng, H., Liang, Q., Abubakar, Y. S., Olsson, S., Zhou, J., & Wang, Z. (2018). The endosomal recycling of FgSncl by FgSnx41-FgSnx4 heterodimer is essential for polarized growth and pathogenicity in *Fusarium graminearum*. *The New phytologist*, 219(2), 654–671. <https://doi.org/10.1111/nph.15178>

SUPPORTING INFORMATION

Additional supporting information may be found in the online version of the article at the publisher's website.

How to cite this article: Rutter, B. D., Chu, T.-T.-H., Dallery, J.-F., Zajt, K. K., O'Connell, R. J., & Innes, R. W. (2022). The development of extracellular vesicle markers for the fungal phytopathogen *Colletotrichum higginsianum*. *Journal of Extracellular Vesicles*, 11, e12216. <https://doi.org/10.1002/jev2.12216>